TKK Dissertations 54
Espoo 2006

LOSS REDUCTION IN COUPLED RESONANCE SURFACE ACOUSTIC WAVE FILTERS OPERATING AT GHZ FREQUENCIES

Doctoral Dissertation

Johanna Meltaus

Helsinki University of Technology
Department of Engineering Physics and Mathematics
Optics and Molecular Materials Laboratory

TKK Dissertations 54
Espoo 2006

LOSS REDUCTION IN COUPLED RESONANCE SURFACE ACOUSTIC WAVE FILTERS OPERATING AT GHZ FREQUENCIES

Doctoral Dissertation

Johanna Meltaus

Dissertation for the degree of Doctor of Science in Technology to be presented with due permission of the Department of Engineering Physics and Mathematics for public examination and debate in Auditorium AS1 at Helsinki University of Technology (Espoo, Finland) on the 8th of December, 2006, at 12 noon.

Helsinki University of Technology
Department of Engineering Physics and Mathematics
Optics and Molecular Materials Laboratory

Teknillinen korkeakoulu
Teknillisen fysiikan ja matematiikan osasto
Optiikan ja molekyylimateriaalien laboratorio

Distribution:
Helsinki University of Technology
Department of Engineering Physics and Mathematics
Optics and Molecular Materials Laboratory
P.O. Box 3500
FI - 02015 TKK
FINLAND
URL: http://omm.tkk.fi/
Tel. +358-9-451 3135
Fax. +358-9-451 3164
E-mail: Johanna.Meltaus@tkk.fi

ISBN-13 978-951-22-8516-7
ISBN-10 951-22-8516-9
ISBN-13 978-951-22-8517-4 (PDF)
ISBN-10 951-22-8517-7 (PDF)
ISSN 1795-2239
ISSN 1795-4584 (PDF)
URL: http://lib.tkk.fi/Diss/2006/isbn9512285177/

TKK-DISS-2221

Otamedia Oy
Espoo 2006

HELSINKI UNIVERSITY OF TECHNOLOGY P. O. BOX 1000, FI-02015 TKK http://www.tkk.fi	ABSTRACT OF DOCTORAL DISSERTATION

Author Johanna Kristiina Meltaus

Name of the dissertation

Loss reduction in coupled resonance surface acoustic wave filters operating at GHz frequencies

Date of manuscript 19.9.2006	Date of the dissertation 8.12.2006
☐ Monograph	☒ Article dissertation (summary + original articles)

Department	Engineering Physics and Mathematics
Laboratory	Optics and Molecular Materials Laboratory
Field of research	Surface acoustic waves
Opponent(s)	Dr. Sylvain Ballandras
Supervisor	Prof. Matti Kaivola
(Instructor)	Docent Victor P. Plessky

Abstract

This thesis discusses loss mechanisms in periodic and quasi-periodic leaky surface acoustic wave (LSAW) coupled resonator filters (CRFs) operating at GHz frequencies and methods to suppress those mechanisms. The work focuses on resistive losses in the interdigital transducer (IDT) electrodes, acoustic loss resulting from conversion of SAW to bulk acoustic waves (BAW) at discontinuities of periodicity, and filter topologies striving for minimizing these mechanisms. Furthermore, losses resulting from acoustic radiation from connecting electrodes (busbars) of IDTs on LSAW substrates are studied.

Novel topologies for low-loss filters at 1–2 GHz frequencies presented in this work comprise (i) two different CRF tracks operating electrically in parallel, (ii) a 5-IDT longitudinal CRF with distributed gaps, and (iii) a double-resonance filter structure proposed here for the first time. In all of the devices, 42°-$LiTaO_3$ is used as the piezoelectric substrate. The operation of the proposed devices is analyzed and their attainable performance is demonstrated with experimental results. Extremely low-loss filter performance with insertion loss on the order of 1 dB is obtained in 2 GHz range with all proposed topologies.

In addition, principles and methods for design and simulation of CRFs is discussed in this thesis, and stochastic (global) optimization algorithms specifically suited for multi-element CRFs are proposed. Furthermore, non-synchronous resonator elements for use with CRFs on leaky substrates are considered, and the effect of contact pad topology on filter performance is discussed based on experimental results.

Keywords Surface acoustic waves, Bandpass filters, Leaky waves, Losses

ISBN (printed)	951-22-8516-9	ISSN (printed)	1795-2239
ISBN (pdf)	951-22-8517-7	ISSN (pdf)	1795-4584
ISBN (others)		Number of pages	87 p. + app. 52 p.

Publisher Johanna Meltaus

Print distribution Helsinki University of Technology / Optics and Molecular Materials Laboratory

☒ The dissertation can be read at http://lib.tkk.fi/Diss/2006/isbn9512285177

TEKNILLINEN KORKEAKOULU PL 1000, 02015 TKK http://www.tkk.fi	VÄITÖSKIRJAN TIIVISTELMÄ

Tekijä Johanna Kristiina Meltaus

Väitöskirjan nimi

Häviöiden pienentäminen kytkettyihin resonaattoreihin perustuvissa pinta-aaltosuodattimissa GHz-taajuuksilla

Käsikirjoituksen jättämispäivämäärä 19.9.2006	Väitöstilaisuuden ajankohta 8.12.2006
☐ Monografia	☒ Yhdistelmäväitöskirja (yhteenveto + erillisartikkelit)

Osasto	Teknillisen fysiikan ja matematiikan osasto
Laboratorio	Optiikka ja molekyylimateriaalit
Tutkimusala	Akustiset pinta-aallot
Vastaväittäjä(t)	Dr. Sylvain Ballandras
Työn valvoja	Prof. Matti Kaivola
(Työn ohjaaja)	Dosentti Victor P. Plessky

Tiivistelmä

Tämä väitöstutkimus käsittelee 1–2 GHz:n taajuusalueella toimivissa periodisissa ja kvasiperiodisissa vuotaviin akustisiin pinta-aaltoihin (LSAW) perustuvissa, akustisesti pitkittäisesti kytketyissä suodattimissa (CRF) esiintyviä häviömekanismeja ja keinoja pienentää niistä johtuvaa vaimennusta suodattimen päästökaistalla. Tutkimuksen painopisteet ovat (i) sormimuuntimissa (IDT) esiintyvät resistiiviset häviöt, (ii) akustiset häviöt, jotka johtuvat pinta-aallon muuntumisesta tilavuusaalloksi kohdissa, joissa rakenteen periodisuus katkeaa, sekä (iii) suodatinrakenteet, joilla pyritään minimoimaan nämä häviöt. Edellämainittujen häviömekanismien lisäksi on tutkittu sormimuuntimien kytkentäelektrodeissa (busbar) tapahtuvasta akustisesta säteilystä aiheutuvia häviöitä.

Tutkittuja akustisia suodatinrakenteita on mallinnettu käyttämällä kytkettyjen aaltomuotojen mallia (COM). Tässä työssä esitellään seuraavat 1–2 GHz:n taajuudella toimivat vähähäviöiset suodatinrakenteet: (i) suodatin, joka koostuu kahdesta rinnankytketystä, keskenään erilaisesta CRF-rakenteesta, (ii) akustisesti pitkittäisesti kytketty, viidestä IDT:stä koostuva suodatin, jossa on käytetty hajautettuja rakoja muuntimien välissä, ja (iii) täysin uudentyyppinen akustiseen kaksoisresonanssiin perustuva suodatinrakenne. Kaikissa tutkituissa rakenteissa pietsosähköisenä alustamateriaalina käytetään 42°-litiumtantalaattia. Kehitettyjen laitteiden toiminta analysoidaan ja niillä saavutettava suorituskyky todennetaan kokeellisin tuloksin. Kaikilla rakenteilla saavutetaan erittäin pienet häviöt, luokkaa 1 dB 2 GHz:n taajuudella. Erittäin vähähäviöisessä viiden IDT:n suotimessa väliinkytkentävaimennus on pienimmillään alle 1 dB, mikä merkitsee huomattavaa parannusta aiemmin raportoituihin vastaavantyyppisiin laitteisiin nähden. Tässä työssä ensimmäistä kertaa raportoitu kaksoisresonanssisuodatin antaa 1.6 GHz:n taajuudella vasteen, jonka suhteellinen kaistanleveys on 1–2% keskitaajuudesta ja väliinkytkentävaimennus päästökaistalla $\sim$ 1.1 dB.

Työssä käsitellään myös CRF-suodattimien suunnittelussa ja mallintamisessa käytettyjä periaatteita ja menetelmiä sekä tässä työssä kehitettyjä CRF-suodattimien optimointiin erityisesti sopivia stokastisia (globaaleja) optimointimenetelmiä. Lisäksi tutkitaan epäsynkronisten resonaattorirakenteiden toimintaa LSAW-alustoilla ja kontaktimetalloinnin vaikutusta suodattimen toimintaan.

Asiasanat Akustiset pinta-aallot, radiotaajuussuodattimet, häviöt

ISBN (painettu) 951-22-8516-9	ISSN (painettu) 1795-2239
ISBN (pdf) 951-22-8517-7	ISSN (pdf) 1795-4584
ISBN (muut)	Sivumäärä 87 s. + liit. 52 s.

Julkaisija Johanna Meltaus

Painetun väitöskirjan jakelu Teknillinen korkeakoulu / Optiikan ja molekyylimateriaalien laboratorio

☒ Luettavissa verkossa osoitteessa http://lib.tkk.fi/Diss/2006/isbn9512285177

Preface

This work was carried out in the Materials Physics Laboratory and in the Optics and Molecular Materials Laboratory at Helsinki University of Technology, Finland, in collaboration with GVR Trade SA, Bevaix, Switzerland, Temex Microsonics (now Temex), Sophia-Antipolis, France, and Samsung Electro-Mechanics Co., Suwon, Republic of Korea. My work was supported by scholarships from the Foundation of Technology, the Finnish Cultural Foundation, Nokia Foundation, Helsinki University of Technology, Finnish Konkordia Fund, Magnus Ehrnrooth Foundation, and Jenny and Antti Wihuri Foundation, for which support I am grateful.

I started my thesis work in the Materials Physics Laboratory under the supervision of Professor Martti Salomaa. Although his untimely passing prevented him from seeing this work finished, I am deeply grateful to him for providing me with the possibility of embarking on this journey, and for all the support he gave me on the way. I finished this work in the Optics and Molecular Materials Laboratory, supervised by Professor Matti Kaivola, and to him I express my deep gratitude for guiding me through the rest of the journey.

My instructor, Victor Plessky, has been the driving force behind the research described in this thesis. His endless flow of new ideas, his optimism and his positive attitude towards life in general and research-related problems in particular have gotten me over many a desperate pitfall along the way. I am also more than grateful for the warm hospitality I had the privilege to enjoy every time I visited Victor and Irina in Switzerland. It has been an honor to work with Victor, and a pleasure.

Throughout the years I have had the privilege of working with many wonderful people. All my friends and colleagues from the times of Materials Physics Laboratory have made my life more interesting and my workdays a source of joy. I had a great time with you. Special thanks to Janne Salo, for the many conversations during coffee breaks, and for the excellent tour of Paris. I also thank Sami Virtanen for his steadfast company during the years in the Lab. My thanks also to my new labmates in the Optics and Molecular Materials Laboratory—it has been a pleasure working with you all.

I would like to extend my warmest thanks to the members of the SAW group, past and present, for everything, from scientific collaboration to the infamous Friday lunch discussions to the open-mindedness exhibited during conference travels, to all the help I received in the dissertation process. Saku Lehtonen, Tapani Makkonen and Jouni Knuuttila paved the way before me, showing how it is done, and with style, too. After they left, Olli Holmgren, Kimmo Kokkonen, and Sanna Härmä have been invaluable

as colleagues and as friends, constituting something that for me is more like a small family than a research group. I owe you all a lot, and I am glad I had the chance to know you and to work with you.

Finally, my loving thanks to my family and my friends, without whom I would not be where I am, nor who I am.

Espoo, November 15th, 2006
Johanna Meltaus

List of Publications

This dissertation is a review of the author's work in the field of surface acoustic wave technology. It consists of an overview and the following selection of publications in this field:

I J. Meltaus, V. P. Plessky, S. Härmä, and M. M. Salomaa, "SAW Filter Based on Parallel-Connected CRFs with Offset Frequencies", *IEEE Transactions on Ultrasonics, Ferroelectrics, and Frequency Control*, accepted for publication.

II J. Meltaus, V. P. Plessky, S. Härmä, and M. M. Salomaa, "Low-Loss, Multi-Mode 5-IDT SAW Filter", *IEEE Transactions on Ultrasonics, Ferroelectrics, and Frequency Control* **52**(6), pp. 1013-1019 (2005).

III J. Meltaus, P. Hämäläinen, and V. P. Plessky, "Design of Coupled SAW Filters Using Genetic and Evolution Algorithms", Report TKK-F-A847 (2006). Submitted to *IEEE Transactions on Evolutionary Computation*.

IV J. Meltaus, S. S. Hong, O. Holmgren, K. Kokkonen, and V. P. Plessky, "Double-Resonance SAW Filters", *IEEE Transactions on Ultrasonics, Ferroelectrics, and Frequency Control*, accepted for publication.

V J. Meltaus, S. S. Hong, and V. P. Plessky, "Acoustic Radiation Losses in Busbars", Report TKK-F-A848 (2006). Submitted to *IEEE Transactions on Ultrasonics, Ferroelectrics, and Frequency Control*.

VI J. Meltaus, S. S. Hong, and V. P. Plessky, "Non-Synchronous Resonators on Leaky Substrates", *Proc. of the 2005 IEEE International Ultrasonics Symposium*, pp. 2153-2156 (2005).

Throughout the overview, these publications are referred to by their Roman numerals.

Author's Contribution

The studies in this dissertation are the result of work carried out in the Materials Physics Laboratory and in the Optics and Molecular Materials Laboratory at Helsinki University of Technology (TKK), Finland, during the years 2001–2006. All Papers were prepared in collaboration with Victor P. Plessky (GVR Trade S.A., Bevaix, Switzerland). Papers I–II involved collaboration with RF SAW Inc., Richardson, Texas, USA. Paper III is co-authored with Perttu Hämäläinen (Telecommunications Software and Multimedia Laboratory, TKK). Papers IV–VI are result of collaboration with Seong Su Hong (Samsung Electro-Mechanics Co., Ltd., Suwon, Korea). Paper IV was prepared in cooperation with Olli Holmgren and Kimmo Kokkonen (Optics and Molecular Materials Laboratory, TKK).

The author has substantially contributed to all research presented in Papers I–VI. She is for a significant part responsible for the design of the devices presented in Papers I–IV and in Paper VI. She has carried out the main part of the simulations and performed a significant part of the analysis of simulated and experimental data in all Papers. All programming related to COM simulations and data analysis was performed by the author. All Papers were written mainly by her. A considerable part of the results covered in Papers I–VI has been presented in the annual IEEE Ultrasonics Symposia; those of Papers II-VI by the author and those of Paper I by V. P. Plessky.

List of Abbreviations

The following abbreviations are used in the overview:

BALUN	Balanced to unbalanced
BAW	Bulk acoustic wave
BW	Bandwidth
COM	Coupling-of-Modes
CRF	Coupled resonator filter
DCS	Digital cellular system
DMS	Double mode SAW filter
DR	Double resonance
DRF	Double resonance filter
EM	Electromagnetic
ES	Evolution strategy
FBAR	Thin-film bulk acoustic resonator
FEM	Finite element method
GA	Genetic algorithm
GPS	Global positioning system
IDT	Interdigital transducer
IE	Impedance element
IF	Intermediate frequency
IL	Insertion loss
LLSAW	Longitudinal leaky surface acoustic wave
LSAW	Leaky surface acoustic wave
MW	Microwave
PB	Passband
PCS	Personal communications system
RF	Radio frequency
SAW	Surface acoustic wave
SB	Stopband
SSBAW	Slow shear bulk acoustic wave
TCF	Temperature coefficient of frequency

Contents

1 Introduction

This thesis work is concerned with surface acoustic wave (SAW) devices, more precisely, with coupled resonator filters (CRF). In modern mobile communications devices, high-performance radio frequency (RF) and microwave (MW) SAW filters are in a key role in both transmission and reception of signals. The rapid evolution of the telecommunications field pushes the performance limits of the existing components, and improved performance is required while operation frequencies are constantly shifting further into the MW region.

The devices studied in this work are based on acoustic waves having localized propagation near the surfaces of solids. SAWs can be utilized in a variety of signal-processing and other applications, such as RF filters, intermediate frequency (IF) filters, identification tags, delay lines, and sensors [1–23]. One of the principal advantages of microacoustics-based components over electromagnetic (EM) components at GHz frequencies is the higher quality factor (Q-factor) achievable with acoustical resonators, which allows low-loss resonator and filter performance with steep transition from resonance or filter passband to rejection band. With the ever-increasing number of applications demanding frequency bandwidth, effective separation of frequency bands with filters having sharp transition characteristics and low loss remains necessary.

Another important benefit of microacoustical devices is the compact device size enabled by the low propagation velocity of the acoustic wave as compared with EM waves, on the order of a few km/s. Consequently, the area of a SAW RF filter chip is typically only a few square millimeters. SAW devices are also well-suited for low-cost mass manufacturing because their fabrication processes are relatively simple and do not require the use of exotic or dangerous materials. Therefore, SAW RF filters meet the market demands for high performance, miniaturization and low cost.

Acoustic waves are comprised of displacements of small volumes of an elastic medium. They can propagate either inside the medium (bulk acoustic waves, BAW) or localized near the surface of the material (SAW), and have displacements in the propagation direction (longitudinal, or compressional, waves) or in the direction perpendicular to the propagation (shear or transverse waves). Acoustic waves propagating on the surfaces of elastic materials were discovered by Lord Rayleigh in 1885 [24]. In SAWs, the main part of the displacement field is localizes in the vicinity of the surface, typically within one or a few wavelengths of the propagating wave.

In piezoelectric materials, the deformation caused by an acoustic wave creates an electric field in the material – this is called the direct piezoelectric effect, discovered by Jacques and Pierre Curie in 1880 [25]. The inverse piezoelectric effect comprises the

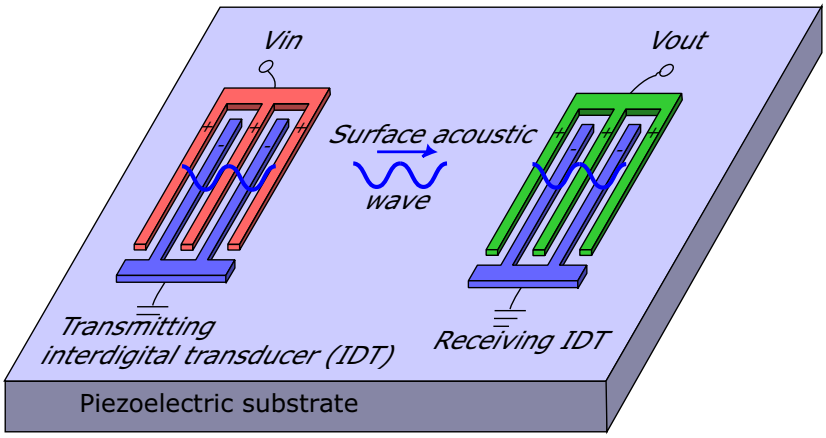

Figure 1.1: Schematic picture of a simple SAW device. The acoustic wave propagating on the surface of the piezoelectric substrate is launched by the input IDT and received by the output IDT.

emergence of deformations in the material under the influence of an applied voltage [26–28]. The inverse piezoelectric effect allows the generation of acoustic waves with an applied electric field, whereas the direct effect enables the reception of waves and the transformation of acoustical energy back to electrical form. SAWs offer, therefore, possibilities in signal processing: electrical signal is converted into an acoustical one, which is mechanically modified and then reconverted back to electrical form. Since the conversion is frequency-dependent, a controlled modification of the original signal is possible.

Direct piezoelectric coupling of RF signal to acoustic surface waves was first reported in 1965 by White and Voltmer [29], when they also proposed a structure to facilitate such conversion, the interdigital transducer (IDT). The discovery of the IDT structure enabled relatively simple yet efficient generation and reception of SAWs and signified a new interest in the applications of acoustic waves. A simple SAW device is schematically illustrated in Fig. 1.1. Interdigital transducers, consisting of two comb-like structures of metal electrodes deposited onto a piezoelectric substrate, act as transmitters and receivers of acoustic waves. An alternating voltage V_{in} is applied to the input IDT, and an output voltage V_{out} is received at the output IDT. A SAW launched by the input IDT propagates under the IDT gratings and on the free or metallized crystal surface between the IDTs. The physics and propagation of surface waves have been extensively studied in several papers and books [30–41].

Of the numerous piezoelectric materials available, quartz was one of the first to be studied. Thanks to its abundance in nature and advantageous materials proper-

ties, such as chemical and temperature stability, it is still one of the most important substrate materials in SAW devices. However, the piezoelectric coupling coefficient of quartz, determining the efficiency of electro-acoustic coupling in the material, is relatively small, and stronger piezoelectric materials, such as lithium tantalate ($LiTaO_3$) [42–48], and lithium niobate ($LiNbO_3$) [49–52], are now commonly used in filter applications that require wide bandwidth and low loss. A number of other substrate materials, such as lithium tetraborate and langasite [53–55], have also been studied. Since piezoelectric substrates typically are anisotropic, different crystal cuts of the same material can have different materials properties. The parameters that govern the acoustic wave generation and propagation in a material, such as the coupling coefficient, the wave velocity, and the propagation loss, can be extracted from measurements [42, 49, 50, 52, 56, 57] or determined theoretically [58, 59].

The size of a SAW component is typically proportional to the acoustic wavelength. The wavelength is inversely proportional to the operation frequency, with the propagation velocity of the wave as the constant of proportionality. As the application frequencies move into the GHz range, the linewidth of SAW structures can approach the limits of optical photolithography used in device fabrication. Therefore, at GHz frequencies, a higher wave velocity is advantageous to keep the structure size within the limits of fabrication technology. Of the existing surface wave types, Rayleigh-type SAW is commonly used in applications. However, its propagation velocity is rather low, approximately 3000 m/s. Therefore, other wave types having higher propagation velocities and subsequently longer acoustic wavelengths are advantageous in high-frequency applications. Such waves include, e.g., leaky and longitudinal leaky SAW (LSAW and LLSAW). Leaky waves, identified by Engan [60], are coupled to slow shear bulk waves (SSBAW) and therefore they leak acoustical energy into the substrate. In certain material cuts, this loss mechanism may be suppressed, and therefore LSAWs can be used also in low-loss applications [47, 61–65]. Recently, much attention has been paid to LLSAWs [66] that have even higher propagation velocity than LSAWs [67–81]. Alternative filter technologies, competing with CRFs at the studied frequencies, include EM filters [82], thin-film bulk acoustic resonators (FBARs) [83], and SAW impedance element (IE) filters [2, 12].

The objective of the research summarized in this thesis is to investigate the loss mechanisms of coupled-resonator-type SAW filters and to improve filter performance in the frequency range of 1–2 GHz. Several important filter specifications fall into this frequency range; in this research, we have worked on the Digital Cellular System (DCS) specification at 1842 MHz, the Personal Communications System (PCS) specification at 1960 MHz, and the Global Positioning System (GPS) specification at 1575 MHz. In

all these specifications, high performance in terms of low loss in the passband and high level of signal suppression elsewhere, as well as small phase and amplitude imbalance in the case of balanced-unbalanced (BALUN) filters, is required. CRFs are capable of meeting all these demands and are, therefore, well-suited for the above-mentioned applications. In this work, methods for reducing losses in the CRF structure are studied. We propose novel filter designs that aim at reducing the insertion loss (IL) in the passband, controlling the filter bandwidth (BW), and improving skirt steepness and out-of-band signal suppression levels.

This thesis is organized as follows: Chapter 2 introduces the concept of a CRF, discusses the basic operation principles of the structure, and the most typical loss mechanisms attributed to it. Acoustic radiation losses from busbars on LSAW substrates, presented in Paper V, are discussed here. Chapter 3 discusses the design methodology for CRFs and explains the simulation methods used in this work. The issue of global optimization of multi-element CRF structures discussed in Paper III is reviewed. Chapter 4 presents the novel filter designs developed in this work (Papers I-II, IV) and summarizes their operation principles and performance. Chapter 5 reviews related results obtained within this thesis work (Papers II, VI).

2 Coupled Resonator Filters

With the emergence of mobile communications systems and the rapid growth and evolution of the field in the early 1990's, the need for wide-band, low-loss, low-cost bandpass filters at GHz frequencies increased substantially. With strong-coupling substrate materials and thick electrodes having high reflectivity, CRFs can answer the needs of the telecommunications industry. They are capable of providing wide-band operation with low losses, combined with signal suppression level that tends to improve with increasing offset from the center frequency. Furthermore, their topology lends itself well for the transformation from unbalanced to balanced electric signal, which is required, e.g., in receiver blocks of mobile phones.

Because of the above-mentioned characteristics, CRF is a popular approach in the design of low-loss filters used, e.g., after the antenna in the reception of RF signals in mobile phones. The performance of the filters is essential for the operation of mobile phone handsets as well as for numerous other applications. This thesis concentrates on the study of the loss mechanisms in CRF structures, aiming to further improve filter performance. In this Chapter, the operation principles of the CRF structure are reviewed, and the principal loss mechanisms affecting it are discussed, including acoustic wave radiation loss from busbars on strong piezoelectric substrates, studied in Paper V.

2.1 Structure and Operation of CRFs

An RF filter provides a frequency response having transmission in the passband of the filter and rejection in the stopband of the filter [82]. A schematic frequency response (attenuation of the electrical signal as a function of frequency) of a bandpass filter is depicted in Fig. 2.1, illustrating the main characteristics of a filter transmission curve. There is some variation in the definition and use of terms associated with filter response; here we introduce some common definitions of terminology used throughout this thesis.

The response of a bandpass filter consists of a passband (PB), the transition bands in which the signal attenuation falls to the required rejection level, and the rejection bands (filter stopband, SB). The width of the PB is typically defined as either the relative (to the minimum IL) BW or the absolute 3-dB BW, often used in the context of RF filters. The IL and the ripple in the PB are important parameters in terms of filter performance.

A longitudinally coupled resonator filter (also referred to as a dual-mode SAW (DMS) filter) consists of acoustical elements that are placed one after another in the

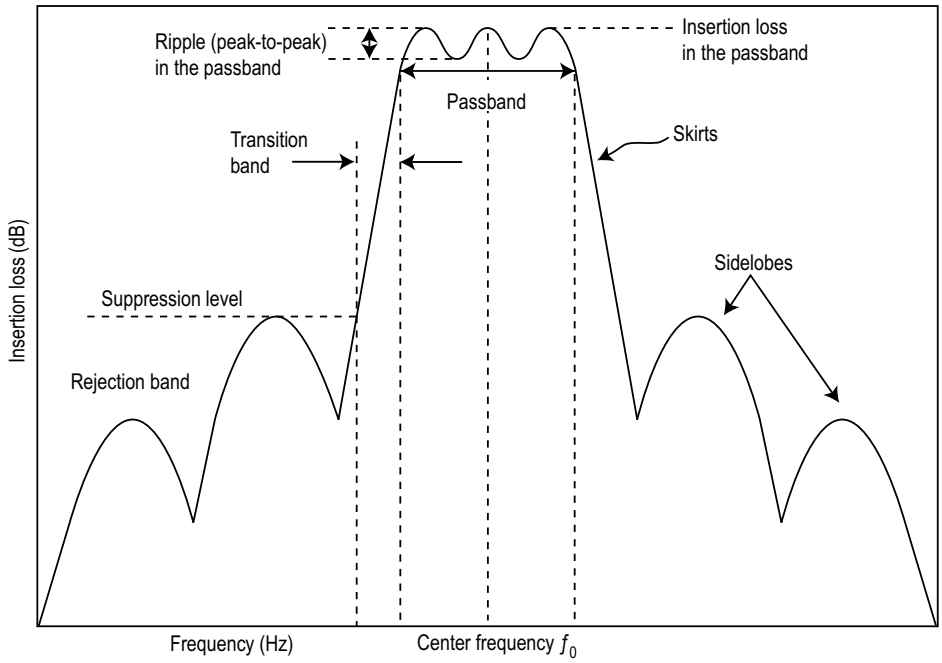

Figure 2.1: Schematic frequency response of a bandpass filter, with definitions for some commonly-used terminology. Important figures of merit include the insertion loss and ripple in the passband, the bandwidth, and the level of signal rejection in the stopband of the filter.

propagation path of the SAW. Such acoustical elements include reflectors, IDTs, and gaps; a schematic of all three elements is depicted in Fig. 2.2. Metal electrodes, or fingers, in the IDT are connected by busbars, and the length over which the opposing fingers of an IDT parallel each other is the aperture, W, of the IDT. The reflector electrodes are typically shorted and connected to the ground to avoid regeneration of SAWs. The period p is defined as the width of one finger, a, and the distance between the fingers; the metallization ratio is a/p. The total length of an IDT or a reflector is here defined as $L = (N-1)p$, where N is the number of fingers in the structural element.

When an alternating voltage is applied over an IDT on a piezoelectric substrate, a SAW having the wavelength $\lambda_0 = 2p$ is generated by the alternating surface charge accumulated on the finger structure. The reflector, as the name implies, reflects the acoustic waves within a certain frequency band around its center (Bragg) frequency, $f_{\mathrm{refl}} = \frac{v}{2p_{\mathrm{refl}}}$, where v is the SAW velocity and p_{refl} is the period of the reflector grating. The frequency band in which reflection occurs is called the reflector stopband and it is not to be confused with a filter stopband. If reflectors are placed at both ends

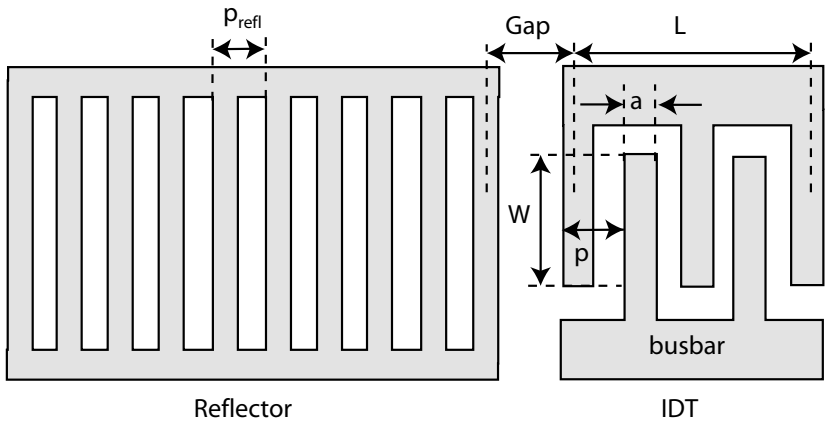

Figure 2.2: Schematic representation of a short-circuited reflector, a gap, and an IDT. Connecting electrodes (busbars) connect the metal fingers in the reflector and in the IDT. The period of the structure is p, and the metallization ratio is a/p. The aperture W of the IDT is the length over which the fingers connected to opposing busbars of the IDT parallel each other.

of the structure, acoustical energy is effectively confined inside the structure within the reflector SB. In CRFs, the gaps serve to provide a controlled phase shift of the propagating acoustic wave.

The principle of a CRF on leaky-wave substrates was first introduced by Morita et al. in [84]. A schematic of a simple 2-IDT CRF is depicted in Fig. 2.3. The structure consists of two acoustically interconnected IDTs, with reflectors at the ends of the device. The electrical frequency response of a CRF results from interfering acoustical resonance modes that arise in the structure. In a symmetrical 2-IDT CRF, the first and the second acoustical modes, schematically represented in Fig. 2.3, are efficiently

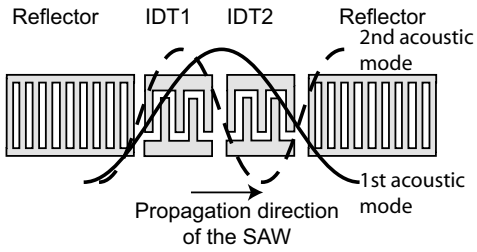

Figure 2.3: Schematic illustration of a 2-IDT CRF structure and the first two acoustic resonance modes arising in it. The acoustic field is distributed over the whole CRF structure, decaying inside the reflectors.

coupled to give electrical response in the output. The larger the number of IDTs in the structure, the higher the order of modes that can be efficiently coupled to input and output. Whereas the period of the IDTs define the operation frequency of the device, their length and the gaps between the elements determine the relative frequencies of the resonances forming in the structure and thereby affect the shape of the frequency response. The aperture, along with the number of fingers in the elements, determine the static capacitance, C_s, of the structure.

To understand the operation of a CRF, the acoustic response of a single IDT to an applied alternating voltage V_0 can be considered. The amplitude of the acoustic wave φ generated by a single IDT at frequency f, ignoring the reflectivity of fingers, is of the form [2, 85]

$$|\varphi| \simeq \frac{K^2 V_0}{2} \left| \frac{\sin\left(\pi \frac{\Delta f}{f_0} \frac{N}{2}\right)}{\pi \frac{\Delta f}{f_0} \frac{N}{2}} \right|, \tag{2.1}$$

where K^2 is the coupling coefficient of the substrate, $\frac{\Delta f}{f_0} = \frac{f - f_0}{f_0}$ is the offset from the center frequency f_0, and N is the number of fingers in the transducer. The center frequency of the IDT is $f_0 = v/\lambda_0$, where v is the SAW propagation velocity in the material.

The response is of the form $|\sin(x)/x|$, with $x = \pi \frac{\Delta f}{f_0} \frac{N}{2}$. The amplitude of the wave is proportional to K^2, and the relative 3-dB BW is $\frac{2\Delta f}{f_0}|_{3dB} \simeq \frac{1}{N_p}$, where $N_p = N/2$ is the number of finger pairs in the IDT.

In the case of multi-IDT CRFs on LSAW substrates, the situation is complicated by internal reflections in the IDTs that give rise to the coupled-resonance behaviour. They also result in the distortion of the initially symmetric $|\sin(x)/x|$ response so that the main lobe peaks at a frequency which is lower than the center frequency of the undistorted response [1].

A simulated electrical frequency response of a simple, symmetric 2-IDT CRF on 42°-$LiTaO_3$ LSAW substrate is presented in Fig. 2.4 with a solid line. The typical features of a CRF response include a low IL in the PB, a relatively large BW, and suppressions that go down to 40–50 dB far away from the PB. The $|\sin(x)/x|$ sidelobes are distinct in the response. The PB is flat, with ripple typically less than 1 dB. The reduced rejection close to the high-frequency end of the PB results from the distorted acoustical response and is inherent to the structure.

Three resonance peaks are revealed in an electrically mismatched situation with the response with source and load impedances changed from 50 Ω to 1 Ω (dashed line in Fig. 2.4). The appearance of the resonances have been analysed in [84] for a 3-IDT case. In a 2-IDT CRF, the strongest resonance at the left edge of the PB results from the second acoustic mode, and the higher-frequency peak corresponds to the first mode. Modifying the length of the gap between the IDTs changes the

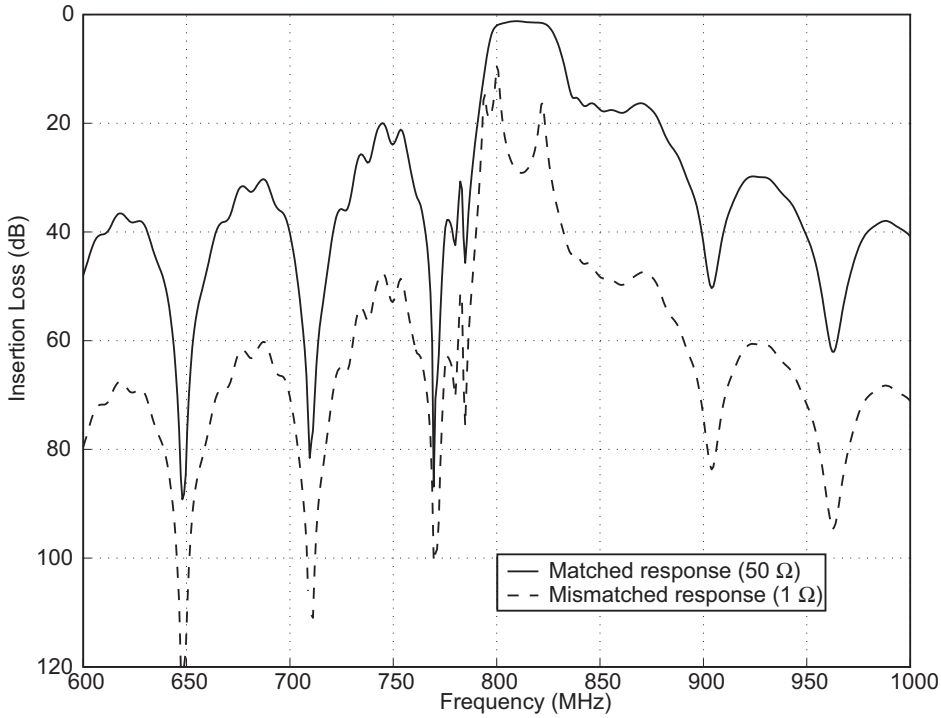

Figure 2.4: Simulated frequency response of a simple 2-IDT CRF. The response in an electrically matched (50-Ω) environment is plotted with the solid line, and a mismatched (1-Ω) response is shown with the dashed line.

frequency of the first mode, thereby changing the frequency difference between the modes and altering the shape and width of the filter PB. Using higher-order modes yields a larger frequency difference between the resonances and allows to achieve a wider PB. Modifying the relative frequencies of the resonances allows tailoring the response of the filter [84, 86–88]. The first small resonance is due to the gap between the reflectors and the IDTs.

2.2 Loss Mechanisms in the CRF Structure

Minimizing the IL in the PB is one of the main objectives of this work. Typically, losses increase with increasing frequency; therefore, controlling the losses is especially important in high-frequency applications. Several loss mechanisms that are due to the CRF structure limit the achievable IL level at GHz frequencies. Some of such loss mechanisms are briefly discussed in the following. Studies of acoustic radiation from busbars, presented in Section 2.2.5, are published in [V].

2.2.1 Resistive Loss

Resistive losses in the metallization are relatively important in CRFs, especially at GHz frequencies. In wide-band devices, the number of electrodes in an IDT tends to be small ($N \sim 20$). In order to have the impedance of the device close to 50 Ω, CRFs typically have rather a wide aperture and therefore long fingers.

The sheet resistance (Ω/square) of a thin conducting film is defined as

$$R_s = \frac{\rho}{h}, \tag{2.2}$$

where ρ is the resistivity of the metal and h is the metallization thickness. Because the current is not evenly distributed over the length of an electrode, the effective resistance for one finger pair can be estimated as [89]

$$R_p = \frac{2}{3} R_s \frac{W}{p \cdot a/p}. \tag{2.3}$$

For an IDT with N_p pairs, the total resistance is R_p/N_p. The aperture W, the period p and the metal thickness h are all proportional to acoustic wavelength. Therefore, $R_p \propto f$, and increasing the operation frequency will increase resistive losses.

To account for the finger resistance in CRF structures, a simple lumped-element model is often used; however, a more complex model is needed to account for the distributed nature of the structure [89, 90].

The larger the number of fingers, the smaller the total resistance of the IDT, since connecting fingers in parallel decreases the total resistance. Reducing the aperture reduces the number of squares, thereby decreasing the resistance. Practical methods for reducing resistive losses in filter structures are discussed in Section 3.1.2.

2.2.2 Propagation Loss

Material losses in the substrate and in the metallization consist of several components. A SAW propagating on a crystal surface is attenuated by interaction with thermal phonons. Phononic loss in metal electrodes is usually higher than that in dielectric crystals.

For LSAW, the propagating wave leaks acoustic energy by coupling to SSBAW. In LSAW cuts of $LiTaO_3$, BAW radiation losses are minimized for free surface on 36°-$LiTaO_3$ and for electrode thickness of 7–10% of wavelength on 42°-$LiTaO_3$. In the case of 42°-$LiTaO_3$, the increased SSBAW radiation loss occurring on free or metallized crystal surface, e.g., in gap regions, can result in a reduced performance of the device.

Other propagation attenuation mechanisms present in SAW devices include air loading and scattering from impurities or from crystalline boundaries.

2.2.3 Conversion from Surface to Bulk Acoustic Wave

A SAW propagating under a grating is reflected from each electrode, and some of the acoustical energy is scattered into the bulk of the substrate. Due to the destructive interference of the BAWs scattered from a periodic grating, the energy loss is effectively suppressed for frequencies lower than the Bragg frequency of the grating, $f_B = \frac{v_b}{2p}$ [2, 91–95], where v_b is the velocity of the bulk wave in the substrate. In this case, energy is stored in the substrate near the grating.

If the periodicity of the grating is broken, the energy-storing effect is reduced and energy is lost to the bulk of the material. Therefore, discontinuities in periodicity, such as gaps between IDTs, add loss and should be avoided. Replacing the physical gaps by short gratings with different periodicity (distributed gaps) allows for significant reduction of losses in RF filters [96, 97].

2.2.4 Radiation of Leaky SAW into Busbars

For leaky SAW, it has been shown that strong frequency-dependent loss may occur in synchronous structures due to radiation of the acoustic wave into busbar region [98–101]. The radiation occurs near the resonance frequency of the structure, below the frequency of bulk wave radiation onset, and is especially strong for long structures. The physics of this effect, first discovered with laser-interferometric measurements of the acoustic field distribution in filters [98], is analyzed in [99, 101]. Radiation occurs if the velocity of the SAW propagating in the grating is such that synchronous coupling to uniformly metallized busbar surface is possible. This effect is pronounced in IDTs with a large number of electrodes and is not usually of concern in conventional CRFs. However, in the novel double-resonance structure described in Chapter 4 it may have a noticeable effect.

2.2.5 Acoustic Radiation from Busbars

Busbar electrodes in SAW devices comprise a network of stray capacitances and resistances, the effect of which can be taken into account by EM simulation. Aside from the resistive losses, the capacitances are typically assumed lossless. However, when a voltage is applied to electrodes on a strong piezoelectric substrate, generation of acoustic waves occurs, and energy is radiated into the substrate in the form of SAWs and BAWs, resulting in losses that can affect the performance of the device.

To estimate this loss mechanism, we have studied systems of 3 busbar electrodes on 42°-$LiTaO_3$ LSAW substrate [V]. Both Finite Element Method (FEM) simulations and measurement results for experimental test structures show that reducing the resistance

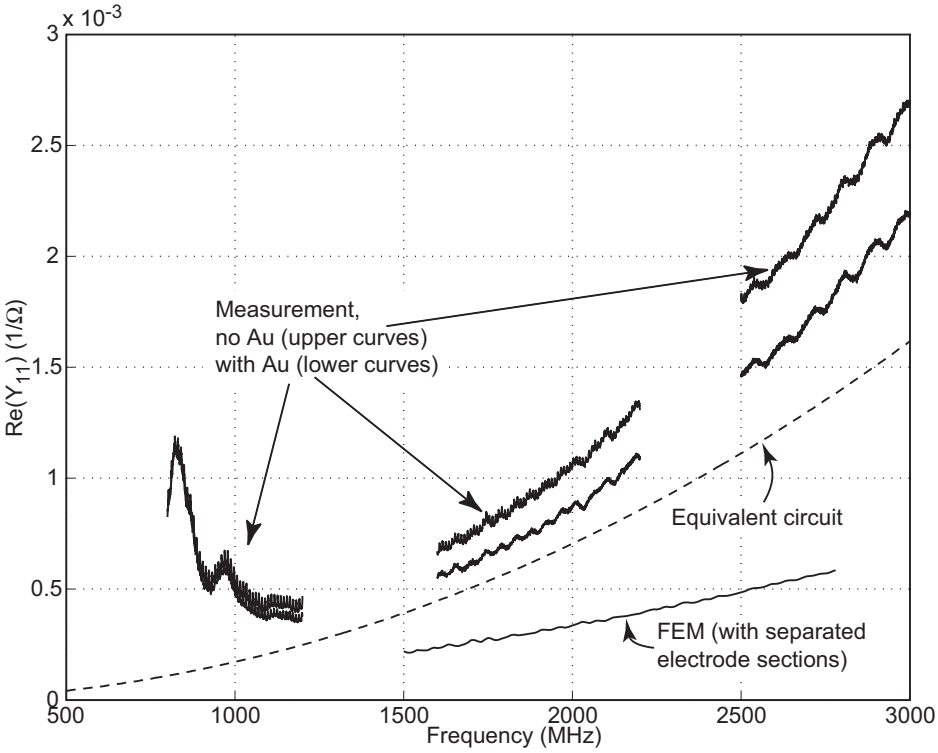

Figure 2.5: Experimental and simulated real part of admittance for long busbar structure. Measurements show higher losses than theoretical models predict. The resonance appearing at 800 MHz is believed to be of EM origin.

of the busbars does not decrease losses in the expected proportion. We associate the remaining losses with the radiation of acoustic waves from the busbar electrodes.

Real part of admittance, corresponding to energy lost in the structure, is presented in Fig. 2.5 for a busbar structure consisting of 3 electrodes with dimensions 100×1500 μm^2. Experimental data in 3 frequency ranges for 160-nm Al electrodes as well as for double-metallized (160 nm Au layer on top of Al) electrodes are shown, along with a FEM simulation and the admittance calculated from an equivalent circuit model. Both theoretical models predict lower losses than those obtained experimentally. Moreover, instead of the expected 50% reduction of losses, the double metallization gives only 20% lower Re(Y) than the single Al layer. This indicates that other loss mechanisms besides the resistive losses are present and have a significant effect.

Both FEM simulations and measurements exhibit low-frequency oscillations that seem to correspond to interference of SAWs generated by the edges of the electrodes. In addition to SAWs, bulk waves are radiated by the structure. These acoustic loss

mechanisms can reduce the Q-factor of the structure significantly. Experimental Q-values as low as ∼10 were observed for long busbar studied here. For a 2-GHz filter with 0.4 pF capacitances parallel to input and output, reducing the busbar Q-value from infinity to 10 results in approximately 0.2–0.25 dB increase in the IL. If the IL level is near 1 dB, this constitutes a significant effect on performance. The final effect on filter performance will be dependent on the topology.

2.3 CRFs vs. Other Filter Technologies

At GHz frequencies, a few alternative filter technologies are used in the same application areas as CRFs. The most prominent of these are probably ladder-type IE and FBAR filters [1,2,102–106]. Although both filter types consist of acoustical resonator elements electrically connected in a ladder network, their acoustical operation principles and fabrication technologies are different. Acoustical impedance elements [12] are based on SAW resonators, whereas the FBAR technology is based on bulk waves.

In certain applications, e.g., in the transmitter of a mobile phone, the filter must be able to withstand high power levels up to 3 W. In such cases, CRFs may not be optimal, as ladder-type IE filters often have a superior power handling capability. Also FBAR filters offer a good power handling capability and fast transition from filter PB to rejection band. Furthermore, their operation frequencies can be extended up to the 10-GHz range [107].

Both IE and FBAR ladder filters suffer from a rejection level that is determined by the capacitance of the resonator network and cannot be easily improved without affecting the IL in the PB. Moreover, the transformation from a single-ended to a balanced signal is not straightforward using ladder networks, whereas with a CRF structure, it can be realized relatively easily.

3 Simulation and Design of CRFs

This Chapter will discuss the design principles of CRFs and review the simulation and optimization methods used in this work. Results for global stochastic optimization of CRFs, published in [III], are presented in Section 3.3.

3.1 Design Considerations

In longitudinally coupled resonator filters, the choice of device parameters is often a compromise between conflicting demands. In addition to the device parameters, the choice of the substrate affects the achievable performance of the filter.

Different types of CRF designs include, e.g., multi-IDT CRFs [90, 108–112], CRFs with multiple tracks [86,87,113–115], and balanced designs [116–118]. Designing CRFs have been studied also in, e.g., [88, 119–121].

3.1.1 Substrate Material

In this work, leaky waves propagating in the X-direction on a 42°-Y-rotated $LiTaO_3$ substrate (42°-$LiTaO_3$) with a metallization thickness relative to wavelength h/λ =8% were used [45–47]. If not otherwise specified, this material is implied as the substrate material henceforth. The choice of the material was determined by the need to obtain both wide-band operation and low IL at relatively high operation frequencies (1–2 GHz). To obtain a wide PB, strong coupling and high reflectivity are preferable. For an IDT without internal reflections, the 3-dB BW is directly proportional to the coupling coefficient, K^2 [12]. The reflectivity of the structure ($N_p\kappa$, where κ is the reflectivity of one period on the given substrate and N_p is the number of electrode pairs) determines the maximum width of the SB of the reflectors. For minimized energy loss, the filter PB cannot be wider than the reflector SB.

The reflectivity κ depends on the thickness and the width of the metal electrodes, increasing with increasing thickness [50,64]. The propagation attenuation also depends on the electrode thickness and on the crystal cut; therefore, it is possible to find a combination of metal thickness and crystal cut having both high reflectivity and low attenuation [47, 122].

The LSAW 42°-YX-cut of $LiTaO_3$ proposed by K. Hashimoto *et al.* [45–47] provides a high coupling coefficient $K^2 \sim 5\%$ with propagation attenuation having its minimum at $h/\lambda = 7\% \ldots 10\%$. Using thick electrodes yields a large κ, enabling a wide PB of typically 3%–5% of center frequency [47, 50, 62, 64, 122]. The LSAW propagation velocity of $v \sim 4$ km/s (under grating) gives an acoustic wavelength of $\lambda = 2$ μm

at 2 GHz, resulting in the critical dimension of 0.5 μm with 50% metallization ratio, which is still realizable using standard photolithography processes.

The main drawback of 42°-$LiTaO_3$ is its poor temperature stability, which is not comparable to, e.g., that of some cuts of quartz [123, 124]. The first-order temperature coefficient of frequency (TCF) of the 42°-$LiTaO_3$ substrate is approximately -40 ppm/°C, which for an operating temperature range of 100 °C at 2 GHz gives 4 MHz temperature tolerances on both sides of the passband. Combined with the fabrication tolerances, the tolerances required on each side of the passband may be as large as 10 MHz. For comparison, the first-order TCF of ST-quartz is zero and the second-order TCF is $-3 \cdot 10^{-2}$ ppm/°C^2, which in the above example would result in frequency tolerances of -0.15 MHz.

3.1.2 Filter Topology

In many applications, the most important characteristic of a bandpass filter is the IL in the PB. Even at high frequencies, a low IL less than 1–2 dB is often required over the total width of the PB. To minimize the IL, the various loss mechanisms discussed in the previous chapter must be suppressed.

A CRF typically has relatively short IDTs, the number of fingers ranging from 10 to 40, and a wide aperture of 50 to 100 wavelengths. As discussed in the previous Chapter, at high frequencies the resistive loss in the metal fingers becomes significant for the device performance. Increasing the number of fingers and decreasing the aperture reduces the resistance of an IDT. For a device matched to a given impedance level (typically 50 Ω for RF filters), for example the following methods of reducing resistive loss can be considered:

1. Connecting 2 identical devices in parallel allows to reduce the aperture in each device by half.

2. Increasing the number of electrodes in an IDT allows both to decrease the aperture and to reduce the role of the resistance. However, often the need for a wide PB limits this possibility.

3. Using a double metallization on busbar electrodes further reduces resistive losses in the device.

All of the above-mentioned methods are implemented in the present research.

Conversion of SAW to BAW at discontinuities in periodicity of the structure results in a loss of acoustic energy that can be critical to device performance. To suppress this loss mechanism, quasi-periodic structures can be utilized [97, 112, 125–129]. In

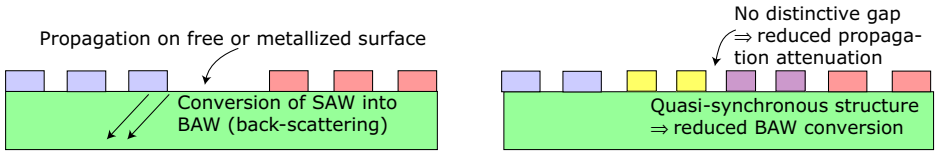

(a) Open-surface gap. (b) Distributed gap.

Figure 3.1: Schematic of a conventional open-surface (a) and a distributed (b) gap design. Using a quasi-periodic structure such as a distributed gap significantly reduces the conversion of SAW into BAW.

this work, a distributed-gap structure (Fig. 3.1) is used to minimize the BAW radiation. In the distributed gap approach, the (typically metallized) gap between the IDTs (Fig. 1(a)) is replaced with short IDT sections having a period different from, typically smaller than, the main IDTs (Fig. 1(a)). The required phase change conventionally obtained with a metallized gap is provided by the change in the finger period. Since abrupt changes in the periodicity are minimized, the conversion of SAW into BAW and, subsequently, losses can be considerably reduced [97, 112]. Moreover, for 42°-$LiTaO_3$, which features minimum attenuation for SAW propagation under a grating, the propagation loss is reduced.

Resulting from the product of the $|\sin x/x|$-type responses of the IDTs (Eq. 2.1), the response of a simple CRF (Fig. 2.4) exhibits rejection levels that increase far away from the PB. The response of the structure features sidelobes the level of which reduces with increasing order. Increasing the number of electrodes in the structure narrows down the sidelobes and accelerates the decay of signal level with respect to frequency.

For 3-IDT CRFs (and the rarely-used 2-IDT structure) the rejection near the high-frequency edge of the PB is reduced. Suppressing this sidelobe can be achieved for example by increasing the number of the IDTs in the structure, thereby increasing the order of interfering acoustic modes and enabling the cancellation of the lobe. An external inductor or capacitor have been proposed so as to increase skirt steepness and to eliminate the sidelobe [111, 130, 131]; however, such external elements add to the complexity of the final design and deteriorate the ultimate achievable rejection level as well as the balance characteristics of balanced devices.

If balanced operation is needed, the role of parasitic capacitances is pronounced. The topology of the filter itself as well as that of the contact pads should be designed such that capacitances that affect the balance characteristics are minimized. Effects of contact pad and package parasitics have been studied, e.g., in [132–134].

3.2 Simulation of CRFs

There are several approaches for simulating SAW devices, both analytical and numerical [119, 135–137]. In this work, we have modelled the devices using the Coupling-of-Modes (COM) model and the transmission matrix representation for the acoustical elements comprising a SAW device. In addition FEM simulations have been used to verify the optimization results obtained using the COM model. Both global and local optimization methods have been employed. A review of modelling approaches of SAW devices can be found in [138].

3.2.1 Coupling-of-Modes Model

The COM model [139–143] is perhaps one of the most powerful and widely-used tools for modelling SAW devices. It is based on representing the surface waves in a uniform periodic structure with two counter-propagating coupled waves, $\varphi_+(x)$ and $\varphi_-(x)$, and analytically solving the system of linear, first-order differential equations describing the mutual interaction of the waves. Excellent papers and books on the COM model and its application in filter design are available [144–154].

A SAW element with a length L is presented in Fig. 3.2. It has acoustic ports at $x = 0$ and $x = L$, the propagation direction of the wave along the x-axis, and one electric port with voltage V and current I. If there are no acoustic waves entering through the acoustic ports ($R(0) = S(L) = 0$), the element can be electrically characterized by a one-port admittance Y relating the voltage and the current,

$$I = YV. \tag{3.1}$$

In practical applications, such an element is used as a building block of more complicated devices, and there are SAWs entering the section. The admittance relation (3.1) is replaced by a more complicated matrix description.

Acoustic amplitudes $R(x)$ and $S(x)$ are slowly varying fields such that

$$\begin{cases} \varphi_+(x) = R(x)\, e^{-j\pi x/p} \\ \varphi_-(x) = S(x)\, e^{j\pi x/p}. \end{cases} \tag{3.2}$$

Assuming the structure in Fig. 3.2 uniform, the COM equations are [143]

$$\begin{cases} \dfrac{\mathrm{d}R(x)}{\mathrm{d}x} = -j\delta R(x) - j\kappa S(x) + j\alpha V \\ \dfrac{\mathrm{d}S(x)}{\mathrm{d}x} = j\kappa^* R(x) + j\delta S(x) - i\alpha^* V \\ \dfrac{\mathrm{d}I(x)}{\mathrm{d}x} = -2j\alpha^* R(x) - 2j\alpha S(x) + j\omega C V. \end{cases} \tag{3.3}$$

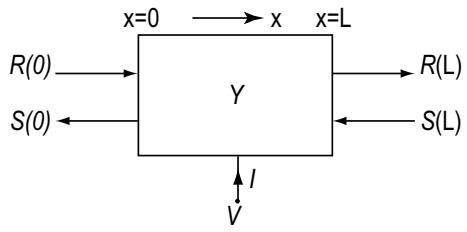

Figure 3.2: A SAW element with length L, having one electric and two acoustic ports. Counter-propagating SAW amplitudes R and S are slowly-varying with respect to the acoustic wavelength. Voltage V is applied to the electric port, giving rise to the current I entering the device. The electrical operation of the device is characterised by the admittance Y.

The material and structure parameters appearing in Eqs. 3.3 are reflectivity per wavelength κ, transduction coefficient α, static capacitance per wavelength C, and surface wave velocity v. In a uniform structure, these COM parameters are constant. Here, the sign of the reflectivity κ is chosen so that it is positive for most commonly-used materials, including the 42°-$LiTaO_3$ used in this work. The detuning parameter δ, determining the frequency offset from the Bragg frequency f_0, is defined as $\delta = \frac{\omega}{v} - \frac{\pi}{p} - i\gamma$, where γ is the attenuation constant and p is the finger period; the acoustic loss term $-i\gamma$ is included in the detuning parameter. A harmonic time dependence is assumed.

Equations (3.3) are somewhat simplified if κ and α are chosen such that they are real-valued – for bidirectional uniform structures, such as simple transducers, this can be done by a translation of the coordinate system [143]. Assuming this and further assuming the structure to be symmetric, solving Eqs. (3.3) with a harmonic ansatz yields

$$R(x) = -\frac{\kappa}{r_0+\delta} S_0 e^{jr_0x} + R_0 e^{-jr_0x} + \frac{\alpha}{\delta+\kappa} V \tag{3.4}$$

$$S(x) = S_0 e^{jr_0x} - \frac{\kappa}{r_0+\delta} R_0 e^{-jr_0x} + \frac{\alpha}{\delta+\kappa} V \tag{3.5}$$

$$\begin{aligned} I(L) &= I(0) + \frac{2\alpha}{r_0}\left(1 - \frac{\kappa}{r_0+\delta}\right)\Big((S_0 - R_0)(1-\cos(r_0x)) - j(S_0+R_0)\sin(r_0x)\Big) \\ &\quad -\frac{4j\alpha^2}{\delta+\kappa} LV + +j\omega CVL, \end{aligned} \tag{3.6}$$

where $r_0 = \sqrt{\delta^2 - \kappa^2}$ and the unknown coefficients R_0, S_0 are determined from the boundary conditions. The total static capacitance of the element is $C_s = CLW$. For

reflectors, Eqs. (3.4–3.5) apply, with the term proportional to voltage V omitted.

The closed-form solution of COM equations enables fast and computationally effective simulation of surface waves, and hence is extremely useful in optimizing SAW devices.

Some Limitations of the COM Model. The COM model is valid for Rayleigh-type SAW and does not take into account effects arising from the leaky nature of the waves propagating on, e.g., 42°-$LiTaO_3$. In order to obtain reliable results for LSAWs, dispersion, scattering and additional attenuation due to energy leaking into the substrate have be incorporated into the model [155–159]. In this work, the approach proposed in [156] was used.

Effects arising from the finite length of gratings are not included in the COM model, which is derived for long, periodic structures. Such effects include, e.g., conversion of SAW to BAW at discontinuities in the periodicity of the device, effects due to electrostatic charge distributions on IDTs and especially at the edges of adjacent IDTs [109, 147, 160, 161], and changes in the phase of the wave. Therefore, for very short transducers, the reliability of the model may be compromised.

Certain parasitic elements affecting the device operation, such as the resistance of the fingers, stray capacitances arising from the topology of the connection pads, and other package-related effects, have to be taken into account outside the COM model. In this work, we added parasitic elements, such as capacitances and finger resistivity, to the total admittance matrix calculated for the structure. To obtain perfect balance, the characteristics of the filter outputs should be exactly similar with respect to input. The COM model does not take into account the polarities of the fingers.

3.2.2 Transmission Matrix Representation

Operation of a SAW device can be described with a matrix representation combining acoustical and electrical effects. A commonly-used form of such a matrix, describing the waves exiting the structure and the current entering the structure with the help of the waves entering the device and the voltage applied to it is called a mixed matrix or a P-matrix [140, 162]. On the other hand, it is possible to construct a transmission matrix that yields the acoustic and electric quantities at the end of the device if the same quantities at the beginning of the device are known [2, 88, 163]. The advantage of the transmission matrix representation is that cascading acoustic elements is straightforward.

In Fig. 3.3 is depicted a structure having 2 acoustic ports and N electric ports, consisting of N acoustically cascaded elements, each of which is represented by a $(2N+$

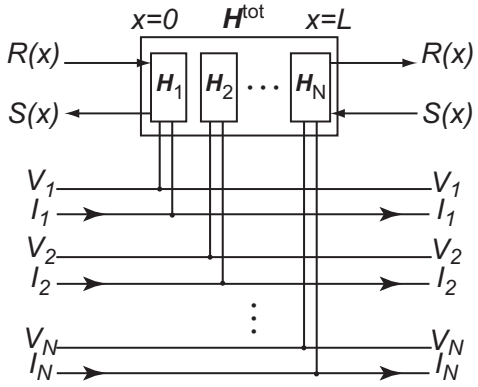

Figure 3.3: A SAW device consisting of N acoustically coupled elements, characterized by transmission matrices $\mathbf{H}_n$. The total structure has two acoustic ports and N electric ports.

$2) \times (2N + 2)$ transmission matrix $\mathbf{H}_n,\ n = 1 \ldots N$. All quantities at the start of the structure ($x = 0$) are assumed to be known. Then, the quantities at $x = L$ may be expressed with a $(2N + 2) \times (2N + 2)$ transmission matrix $\mathbf{H}^{\text{tot}}$ as

$$\mathbf{A}(L) = \mathbf{H}^{\text{tot}}_{(2N+2)\times(2N+2)}\, \mathbf{A}(0), \tag{3.7}$$

where

$$\mathbf{A}(x) = \begin{pmatrix} R(x) & S(x) & V_1(x) & I_1(x) & \cdots & V_N(x) & I_N(x) \end{pmatrix}^T. \tag{3.8}$$

The total transmission matrix $\mathbf{H}^{\text{tot}}$ is constructed from the element matrices $\mathbf{H}_n$ by multiplication.

Coefficients R_0 and S_0 may be solved from Eqs. (3.4)–(3.6) with the help of $R(0),\ S(0),\ V(0)$ and $I(0)$. A straightforward calculation yields the elements of $\mathbf{H}_n$. For the form of $\mathbf{H}_n$ and for formulas of its elements, see [164].

Transmission matrices offer a straightforward way of simulating multi-element devices cascaded from multiple acoustical elements. However, matrix multiplication requires a lot of computer time; therefore, the calculation of transmission matrices can be more time-consuming than using, e.g., P-matrices. Another drawback is that for very long structures or high reflectivity values, the evaluation of the matrix elements may require high-precision calculation.

Admittance Matrix for the Filter. The admittance matrix $\mathbf{Y}_{N\times N}$ of a cascade such as depicted in Fig. 3.3,

$$\mathbf{I} = \mathbf{Y}_{N\times N}\mathbf{V}, \tag{3.9}$$

where $\mathbf{I}$ is the current vector and $\mathbf{V}$ the voltage vector of the N-port structure, is obtained from the transmission matrix $\mathbf{H}^{\text{tot}}$ (Eq. 3.7) by imposing the boundary conditions

$$\begin{cases} S(L) = 0 \\ R(0) = 0 \\ I_{1\ldots N}(0) = 0. \end{cases} \tag{3.10}$$

That is, no waves enter the cascade from either side, and no currents are entering from the left.

Then, $S(0)$ may solved as

$$S(0) = -\frac{1}{H_{22}^{\text{tot}}} \sum_{n=1}^{N} H_{2\,(2n+1)}^{\text{tot}} V_n(0) \tag{3.11}$$

With Eqs. (3.7) and (3.11), the elements of the total admittance matrix are then

$$-Y_{nm} = -\frac{H_{(2n+2)\,2}^{tot}}{H_{22}^{tot}} H_{2\,(2m+1)}^{tot} + H_{(2n+2),(2m+1)}^{tot} \tag{3.12}$$

Simulation of SAW Amplitude. The cascaded structure is characterised by its transmission matrix $\mathbf{H}^{\text{tot}}$ (Eq. 3.7) and an admittance matrix $\mathbf{Y}$ (Eqs. (3.9), (3.12)). For a cascade with N electric ports, the distribution of the slowly-varying amplitudes $R(x)$ and $S(x)$ along the structure can be extracted from the element transmission matrices $\mathbf{H}_n$.

Of the values of acoustical and electrical quantities at the beginning of the cascade, the input voltage $V_{\text{in}}(0)$, applied for example to port 1, may be taken arbitrary or given. In addition, boundary conditions of Eqs. (3.10) apply. Assuming a situation where all the other ports except the input are open-circuited, i.e., $I_{2\ldots N} = 0$, and the input is ideally shorted ($R_{\text{in}} = 0$), the voltages $V_{2\ldots N}(0)$ can be solved from Eq. (3.9). Then, $S(0)$ can be solved from Eq. 3.11. Ignoring the input resistances in the ports results in ideally deep zeros and underestimated losses.

SAW amplitudes R and S at the beginning of each element can be calculated using the cascaded H-matrix of the preceding elements and the values of acoustical and electrical quantities at the beginning of the cascade. For each element, $R(x)$ and $S(x)$ at each point x inside the element can be calculated using the transmission matrix $\mathbf{H}_n$ of the element.

The described procedure gives the correct phase of the SAW in the center of every second electrode. The final amplitude is obtained by the sum of Eqs. (3.2).

3.3 Global Optimization of Multi-Element CRF Structures

In a multi-IDT CRF, especially if multiple tracks are used, the number of device parameters that have to be optimized simultaneously can easily exceed 20 – in a symmetric, single-track, 5-IDT filter with distributed gaps, the number of optimized parameters is 18. The objective function shape can be a complicated function of the parameters, featuring multiple local minima and depending more strongly on some parameters than on others. In such a case, a typical gradient optimization is extremely sensitive to the initial guess of parameters and is prone to converging to a local minimum. Performing several optimization runs with different starting points can help to find a better solution, but such manual iteration is often time-consuming.

In the optimization of SAW devices, we have used the gradient-based optimization functions provided in Matlab. They are efficient tools when the designer has a solid understanding of the structure and hence a good initial guess of the parameters. As an alternative, we have studied stochastic optimization methods [165–169], such as genetic algorithms and evolutionary optimization. Stochastic methods aim at a global search of the whole parameter space, starting from a random situation. Each iteration step is based on the solutions created in the previous step, but the method of proceeding from one step to the next is in some way arbitrary. The random element increases the probability of finding the global minimum. Even though there is no guarantee of converging to the global minimum, the final solution is not dependent on the initial guess of parameters.

Global optimization methods have been applied to the design of SAW devices [170–179]. In this work, stochastic algorithms in the context of 5-IDT CRF optimization were studied. A genetic algorithm (GA) and an evolution strategy (ES) were developed [III]. The ES strives to taking into account the dependence of the objective function on the different parameters by calculating the covariance matrix for the parameters [180], whereas the GA produces the offspring sample randomly from the parent samples.

The algorithms were applied to the optimization problem of a 5-IDT CRF (Section 4.2) with 14 independently optimized parameters. The convergence of the optimization (average of 5 runs), with an objective function that was to be minimized, is shown in Fig. 3.4. In the objective function, important performance parameters such as deviation from specification, curvature in the PB, ripple balow, in, and above PB, and total size of device, were taken into account. The initial convergence of the GA is faster, but the final result produced by the ES has a lower objective function value. However, both algorithms reach a satisfactory result already after 6 generations. Typical frequency responses of the optimized filter at several stages of optimization (shown with circles in Fig. 3.4) are depicted in Fig. 3.5. The final optimization results are

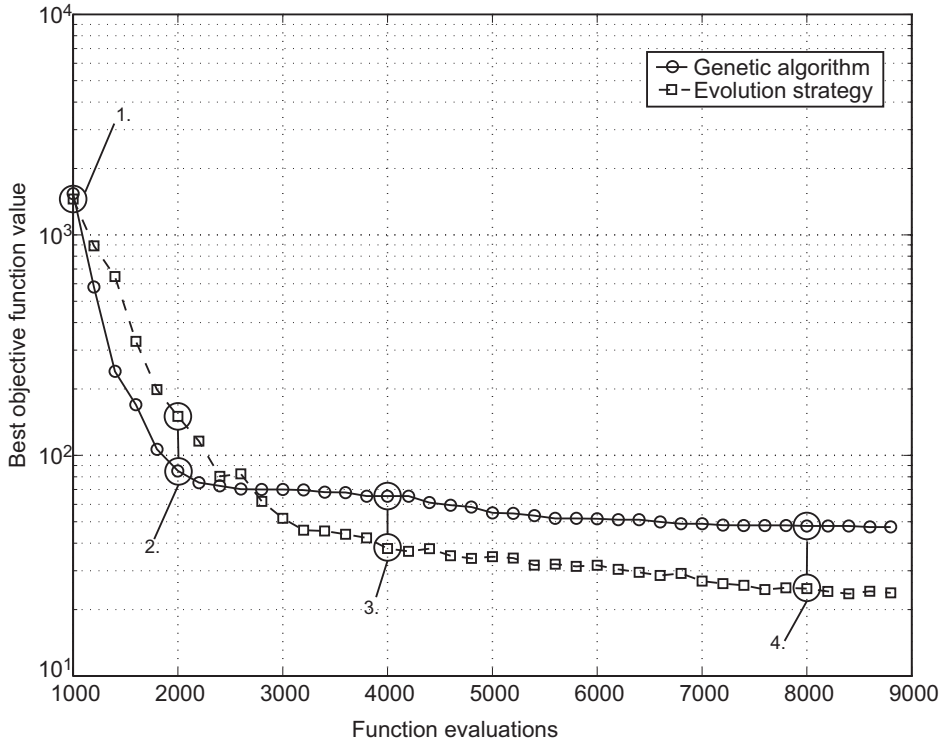

Figure 3.4: Convergence of the stochastic algorithms for a 5-IDT CRF optimization problem. The initial convergence is rapid for both algorithms. The ES reaches a slightly better final solution. The numbers refer to typical frequency responses presented in Fig. 3.5.

comparable.

The computationally demanding covariance matrix calculation used in the ES can limit the general applicability of the algorithm. However, since in CRF simulation with transmission matrices, the matrix multiplications performed during the objective function evaluation constitute the most time-consuming part of the optimization process, the slowness of the ES has no significance in the total time required by the process. Therefore, we deem the ES especially well-suited for CRF optimization.

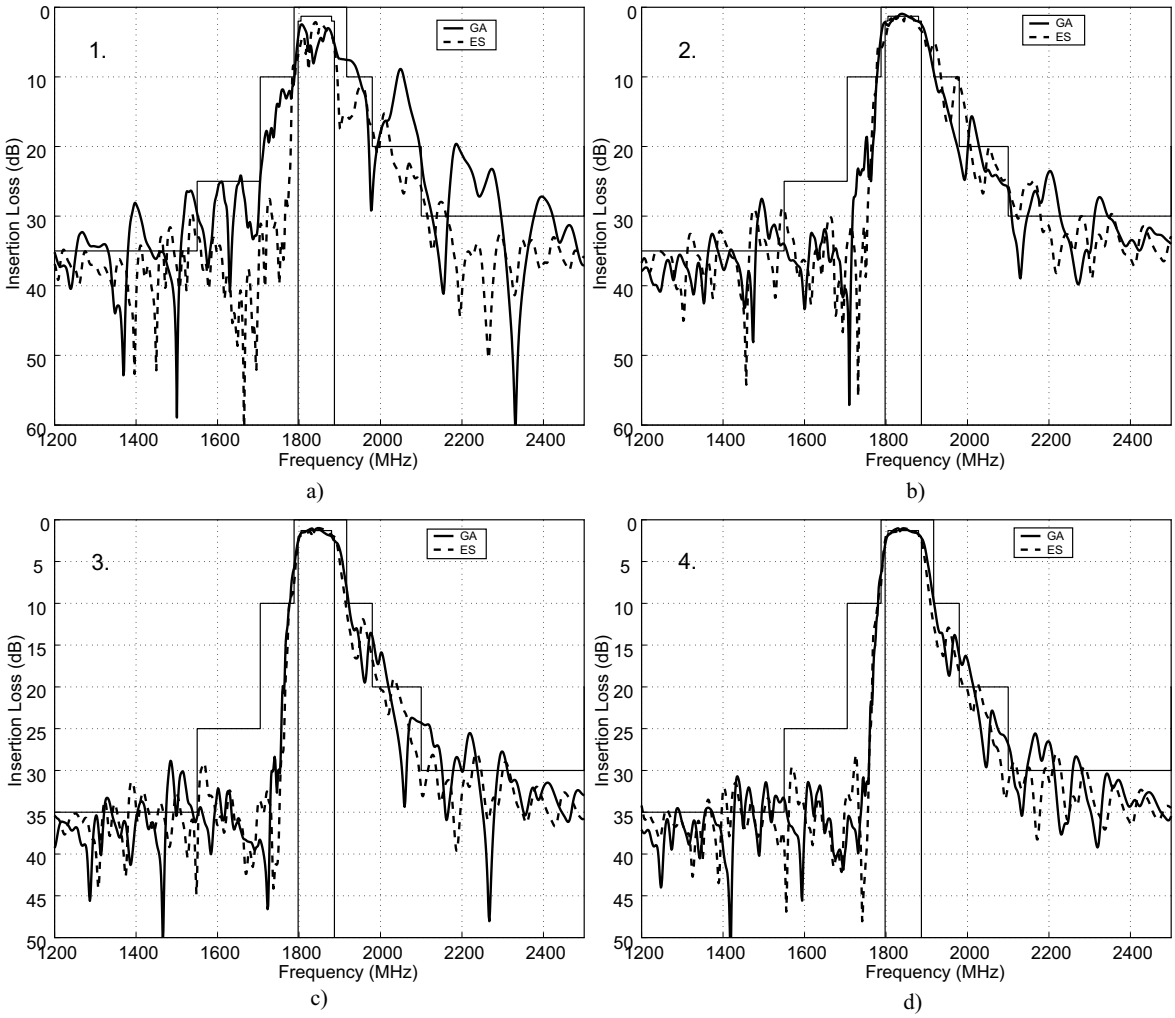

Figure 3.5: Intermediate optimization results (typical frequency responses of the optimized structure) for the GA (solid line) and the ES (dashed line) at points depicted in Fig. 3.4 (after 1000, 2000, 4000 and 8000 function evaluations). Both algorithms obtain a satisfactory result already after 6 generations (2000 function evaluations).

4 Novel CRF Designs: Results and Analysis

In this section, novel device designs developed within this Thesis work and described in Papers I–II and IV are presented. For each topology, the structure and its operation principle are shortly discussed, along with its design objectives. Thereafter, the experimental results for the design are summarized.

In all of the designs described in this section, the substrate material is 42°-rotated YX-$LiTaO_3$.

4.1 Two Different CRF Tracks in Parallel

4.1.1 Main Design Concepts

As discussed earlier, connecting two identical filter tracks in parallel allows to divide the aperture between the two tracks, thus reducing the resistive losses in the electrodes approximately to half of the original value. However, in all other performance aspects the filter will be identical to the corresponding 1-track device. The design approach adapted here [I] strives for extracting further performance improvement from the parallel-track topology by using two different CRF tracks. In such a device, each track is essentially a filter with a narrow bandpass response, and the total response of the device is compiled from the individual track responses. As the bandwidth of the individual tracks is narrower than the one required for the total device, the number of fingers in each track can be increased, which both decreases resistive losses and allows further reduction of the aperture. Alternatively, an extremely wide PB can be synthesized from the track responses.

If the responses of the tracks cancel each other in the filter SB, improved rejection levels can be obtained. With identical filter tracks, this effect is impossible to achieve. For the design approach studied here, the phases of the individual frequency responses of the tracks can be tailored such that in the PB, the responses are in phase with each other, whereas in the SB, they are out-of-phase. Consequently, the track responses can have relatively poor rejection levels as long as they are conveniently cancelled in the final device response. The desired phase response is brought about by inverting the phases in the track outputs with respect to each other. Thereafter, the responses of the tracks can be constructed such that the resonance modes arising in the CRF tracks (see Fig. 2.4) are in-phase in the filter PB [84, 86, 87].

With 3 IDTs, the topology also lends itself extremely well to balanced-output operation. Inverting the polarities of the output IDTs of a track with respect to each other yields a balanced output signal, with a simple interconnection topology.

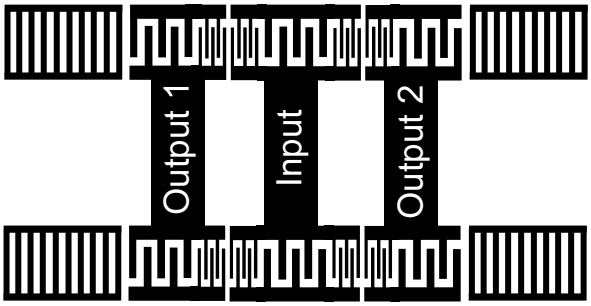

Figure 4.1: Schematic representation of a filter with two different CRF tracks connected in parallel. The phases of the output IDTs are opposite both within the tracks and from one track to the other. Distributed gaps are used instead of metallized gaps.

4.1.2 Structure of the Device

The structure consists of two parallel-connected tracks such as shown in Fig. 4.1 for a 3-IDT device. The polarity of the output IDTs is inverted both within one track (between output 1 and output 2) and between the tracks. Distributed gaps (Fig. 3.1) are used in order to minimize losses due to scattering into BAW.

The final response of the device is composed of the individual track responses, as illustrated with a COM simulation in Fig. 4.2 for a device operating at 880 MHz. The rejection levels of the individual tracks are significantly lower than when connected in the final device, especially near the low-frequency side of the PB. It should also be noted that the transition band steepness is improved compared to a single-track design.

4.1.3 Experimental Results

Devices having 2 or 3 IDTs, both with metallized and distributed gaps, were fabricated and measured. Fig. 4.3 shows the measured frequency response of a two-track CRF with the 3 IDTs separated by distributed gaps, operating at 1960 MHz. The absolute 3-dB BW is 80 MHz (3.1 %) and the minimum IL is 1.3 dB, which is an excellent value for a 2-GHz filter. The measured balance characteristics for amplitude and phase are presented in Fig. 4.4.

For the corresponding metallized-gap devices, the achieved 3-dB BW is 73 MHz (3.7%) and the minimum IL is 1.0 dB. However, the typical IL is not as low as for distributed-gap devices.

Since each of the tracks provides half of the final PB, shifting the response of either track in frequency results in a notch in the PB, as illustrated in Fig. 4.5 for a metallized-

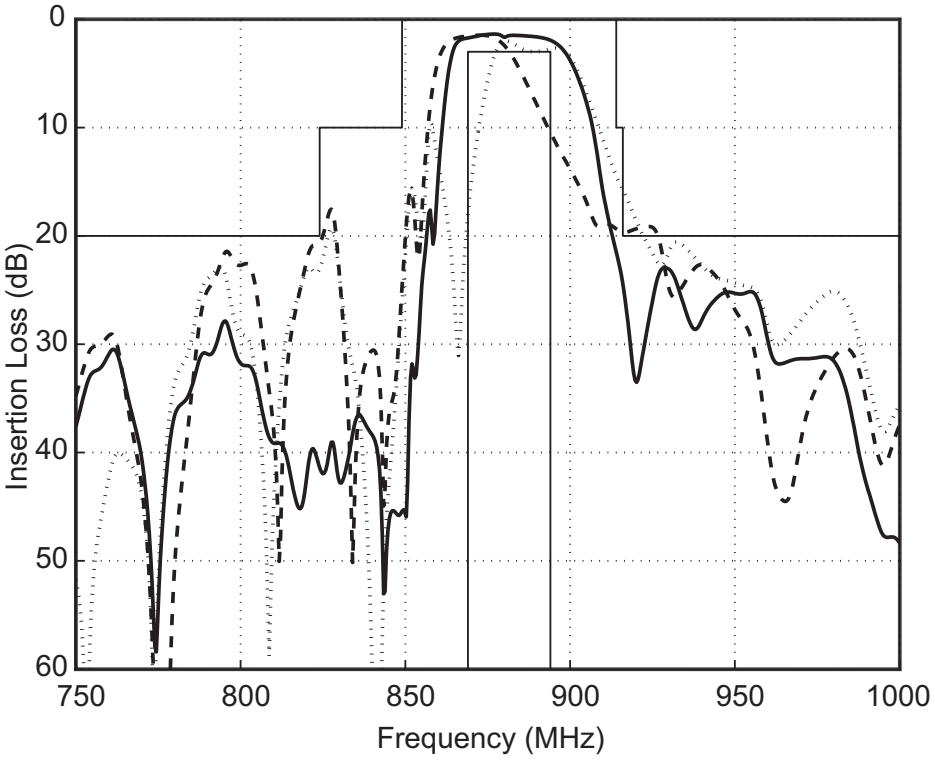

Figure 4.2: Simulated frequency responses of the individual tracks (dashed and dotted curves) and the final device response (solid line) at 880 MHz, illustrating the operation principle of the dual-track device. In the PB of the filter, the responses of the tracks are in phase, whereas in the SB, they are out-of-phase, thereby canceling each other.

gap device operating at 880 MHz. Likewise, to obtain cancellation of the two transfer functions in the filter SB, the responses of the tracks must be accurately tailored. In this type of device, the gaps between the transducers, or in the case of distributed-gap design, the periods in the short IDT sections, determine the center frequency of the track response and therefore control the shape of the final PB. The periods of the main IDTs mainly affect the shape of the transfer function and principally alter the final suppression levels of the device.

4.1.4 Comments and Conclusions

The connection of 2 different CRF tracks in parallel was studied for the first time on strong piezoelectric substrates and for wide-band, low-loss RF filters at 2-GHz frequencies. Similar approaches reported earlier were proposed for narrow-band IF

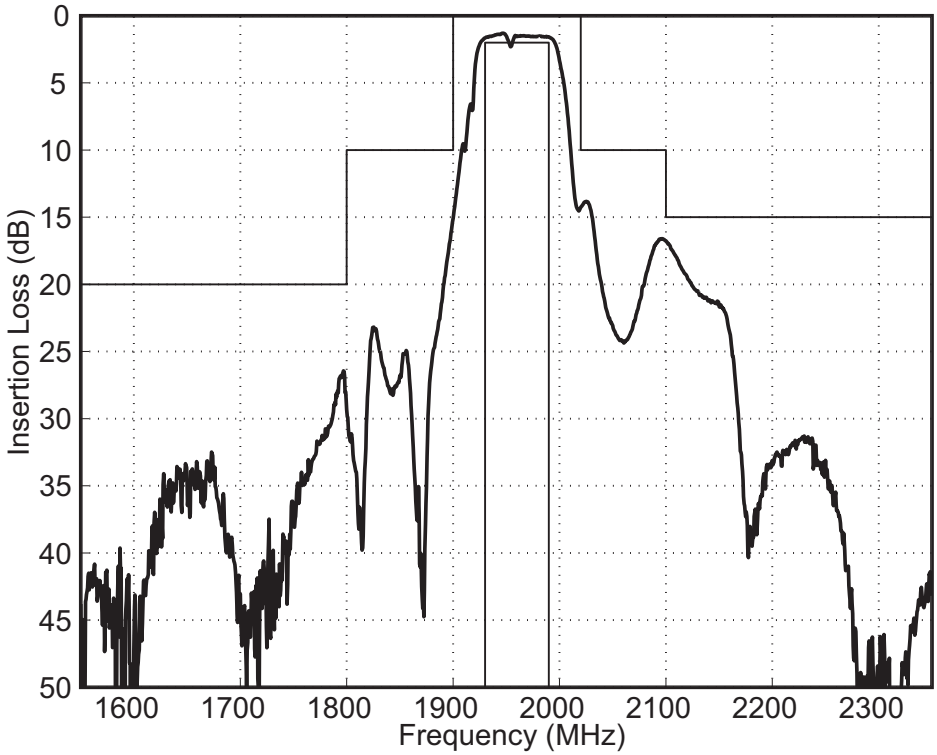

Figure 4.3: Measured frequency response of a 3-IDT parallel-track filter with distributed gaps. The minimum insertion loss in the PB is 1.3 dB and the BW is 3.1% of the center frequency.

filters on quartz [86, 87]. The approach investigated here enables a very low IL in the PB, demonstrated with measurements for an RF filter operating at 1960 MHz. Furthermore, the close-in rejections can be controlled and radical improvements can be obtained in a limited frequency band. To avoid the appearance of a notch in the center of the PB, resulting from the merging of the individual track responses, an accurate adjustment of the IDT periods is necessary. The structure can be used for balanced-output operation; however, it is not ideal for minimum imbalance, as the topology of the outputs is not identical with respect to the input. Although stray capacitances arising between the IDTs will inevitably affect the balance characteristics, it should be possible to improve balanced performance with design modifications.

This approach is especially suitable for very wideband filters for which the specifications on imbalance are secondary to the BW and loss.

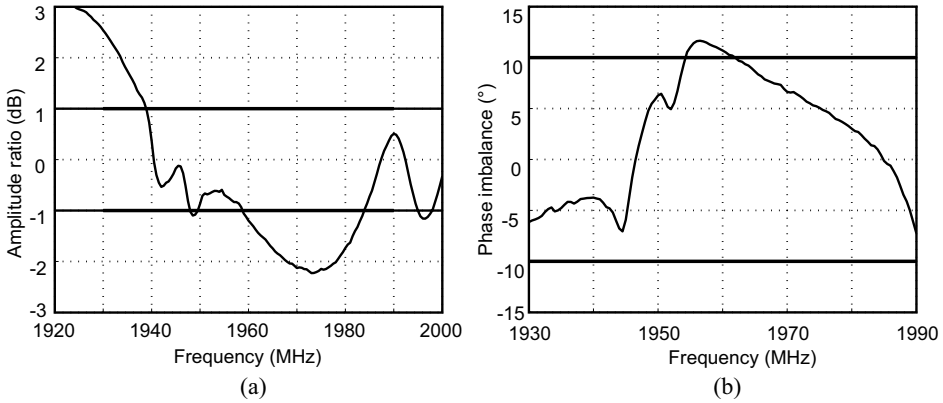

Figure 4.4: Measured balance characteristics of a 3-IDT parallel-track filter with distributed gaps: amplitude (a) and phase (b) imbalance in the filter PB.

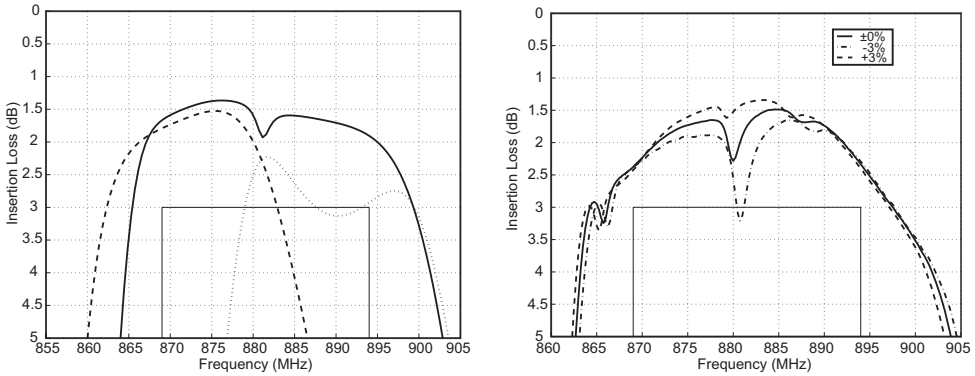

Figure 4.5: Shifting the responses of the individual tracks results in a notch in the total response of the device. (a) Simulated responses of the two tracks and the corresponding total response of a device with metallized gaps. The length of the gap between the IDTs was decreased by 3% from optimum in both tracks, leading to the appearance of the notch in the center of the PB. (b) Experimental results for varying the length of the gaps by ±3%.

4.2 CRF with 5 Main IDTs and Distributed Gaps

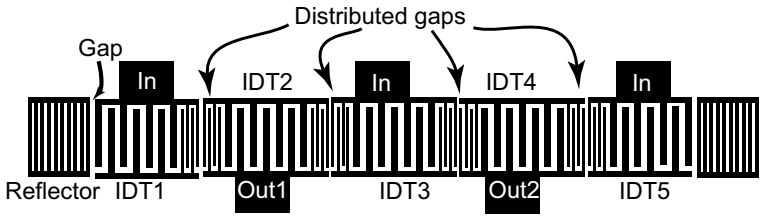

Figure 4.6: Schematic picture of a 5-IDT CRF with distributed gaps.

4.2.1 Design Objectives and Structure

The 5-IDT structure is a logical step in the development of CRF devices [90, 108, 111]. It can be considered as 2 parallel-connected CRF tracks that are placed in the same acoustical channel. In order to obtain wide-band, low-loss performance, a filter with 5 IDTs and distributed gaps was designed (Fig 4.6) [II]. The filter topology contributes to the objective in several ways. Distributed gaps reduce the propagation and bulk-wave conversion loss, yielding improvement in the IL level compared to metallized gaps. Utilizing 5 IDTs allows for a narrower aperture than, e.g., in a 3-IDT filter, reducing resistive loss and thereby further improving the IL. Increased order of acoustical modes arising in the 5-IDT structure enables a wide PB and fast transition to the rejection band, specifically facilitating the suppression of the characteristic sidelobe on the high-frequency side of the PB (Fig. 2.4). Optimizing the interference of SAWs generated by the IDTs, higher rejection levels than with 3-IDT CRF can be obtained. Finally, the topology allows for a simple way of obtaining balanced output by connecting input to the first, third and fifth transducer and inverting the phases of the output transducers (second and fourth) with respect to each other.

4.2.2 Experimental Results

Measured frequency response of the device operating at 1842.5 MHz (handset receiver DCS band) is shown in Fig. 4.7 along with a COM simulation, and measured balance characteristics are depicted in Fig. 4.8. The minimum IL is less than 1 dB and the absolute 2.5-dB BW is 83 MHz (4.5 %), with an extremely flat PB. Suppressions go down to −40-dB level. The amplitude imbalance in the PB ranges from 0 to 1 dB and phase imbalance from −5° to 8°.

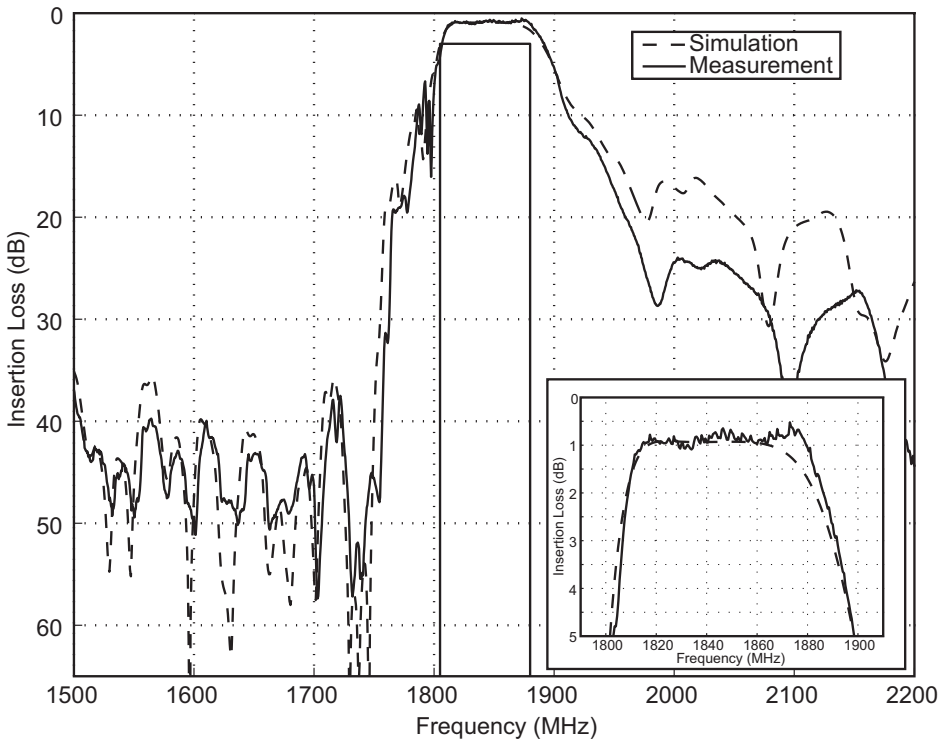

Figure 4.7: Experimental and simulated frequency response of a 5-IDT filter with distributed gaps. The minimum IL is 0.8 dB and the absolute 2.5-dB BW is 83 MHz (4.5%).

The effect of contact pad topology on the filter response and balance characteristics will be discussed in Section 5.2.

The 5-IDT design yields excellent results, combining low losses and high rejection levels. It can replace conventional 3-IDT CRFs, especially if flip-chip technology is used to simplify electrical interconnections.

4.3 Double-Resonance Filter

4.3.1 Objective and Structure

The BW of a CRF is basically determined by the coupling coefficient, K^2, of the piezoelectric substrate, as discussed in the preceding chapters. It is difficult not only to increase the BW but also to decrease it, simultaneously retaining a low IL and a good shape of the transmission curve. Therefore, the design of low-loss filters having 1% to 2% relative BW can be difficult, as suitable substrate materials are not readily available. To obtain narrow-band filter performance on LSAW substrates with strong

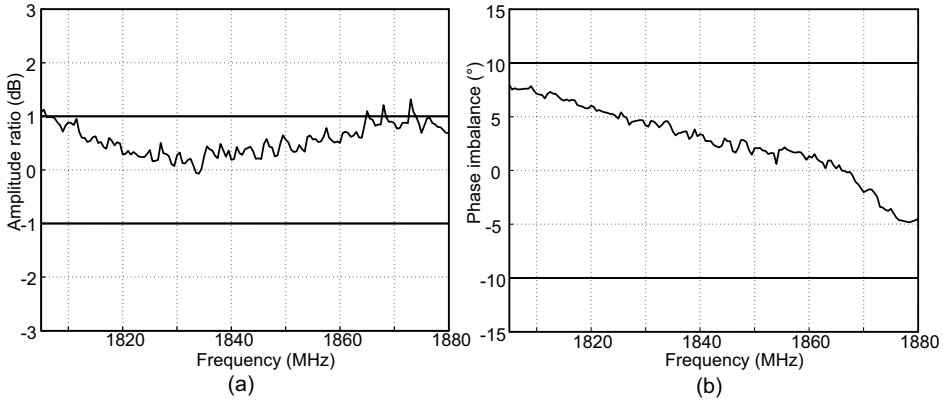

Figure 4.8: Experimental balance characteristics of a 5-IDT filter: amplitude (a) and phase (b) imbalance in the filter PB.

coupling, a novel filter structure such as illustrated in Fig. 4.9(a), was studied [IV]. It consists of IDTs that are long compared to those of conventional CRFs, with the number of fingers N in one IDT significantly greater than $1/K^2$ and $1/\kappa$ – for 42°-$LiTaO_3$, $N \gg 50$. Distributed gaps replace conventional metallized gaps. A similar structure with metallized gaps was previously proposed [181], but experimental results were not satisfactory.

The operation principle of the structure differs from that of the conventional CRFs. As the high reflectivity of the long IDTs makes the propagation of SAW from one IDT to another virtually impossible, no resonance modes are developed over the whole structure. Instead, two distinct resonances arise in the structure: a mode typical of synchronous resonators, arising in the long IDT structure, and a resonance strongly localized in the gap region, similar to hiccup resonance arising in a $\lambda/4$ cavity in a synchronous structure [5, 142] – hence the name "double resonance" filter (DRF). The resonance in the gap serves to transfer acoustic energy from input to output. Consequently, it is critical to minimize the loss occurring in the gap. The unacceptably high losses in early experiments [181] were probably due to energy loss in conventional gaps.

To gain insight into the operation of the structure, the acoustic amplitude distribution in a one-port device (input and output of Fig. 4.9(a) connected in parallel) was studied both theoretically (Fig. 4.9(c)) and experimentally (Fig. 4.9(b)). The experimental amplitude data was obtained with laser-interferometric measurements [182]. Both simulated and experimental results show the synchronous resonance around 1560 MHz and the hiccup resonance at 1600 MHz. Simulations are in excellent agreement with the measurement results.

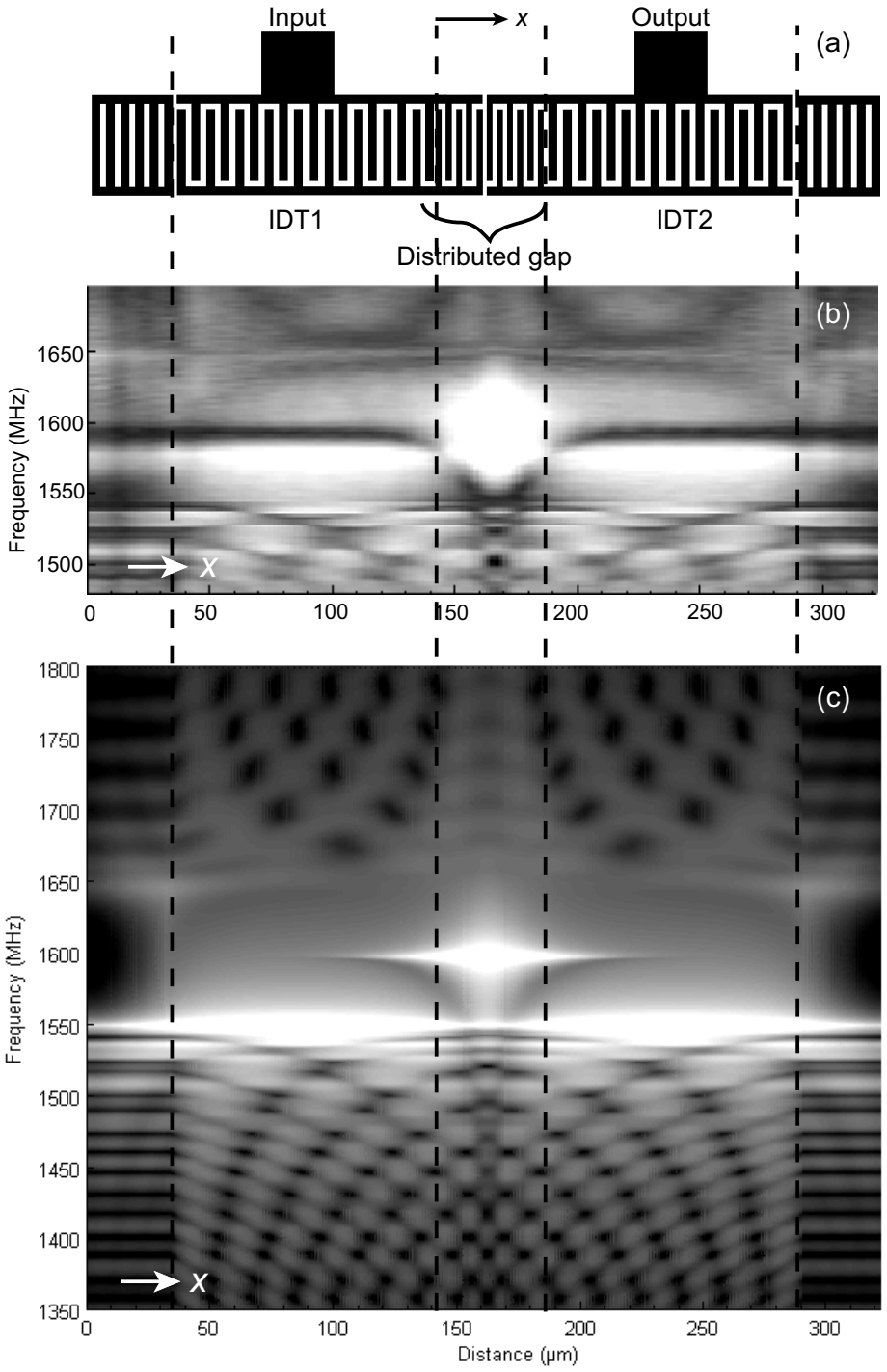

Figure 4.9: (a) Structure of a two-port DRF. The IDTs are considerably longer than in conventional CRFs. (b) Experimental acoustic amplitude distribution in a one-port DR resonator (input and output in (a) connected in parallel) as a function of frequency. (c) Simulated (COM) acoustic amplitude distribution in a DR resonator as a function of frequency. The synchronous resonance is seen at 1560 MHz and the hiccup resonance at 1600 MHz.

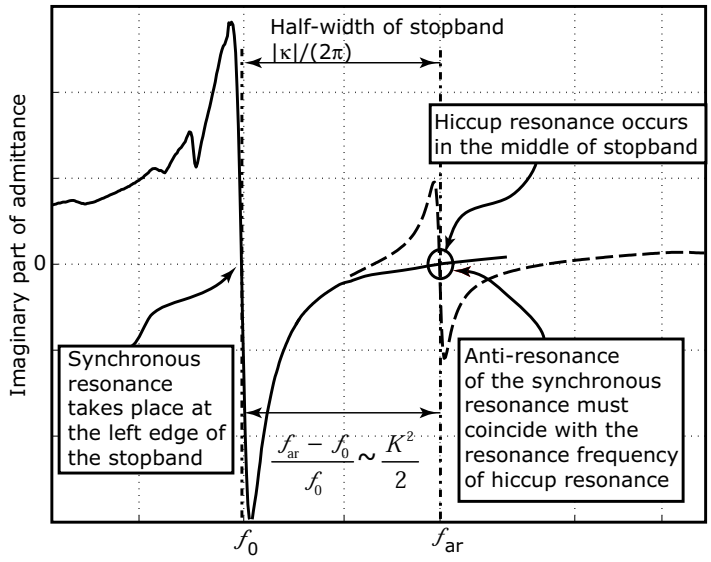

Figure 4.10: Schematic illustration of the self-matching in a DR structure. Self-matching occurs when the anti-resonance frequency of the synchronous resonance and the resonance frequency of the hiccup resonance coincide, and the synchronous resonance acts as a matching inductance for the hiccup resonance.

4.3.2 Self-Matching

It is possible to intrinsically match the hiccup-type resonance arising in the gap of a DR structure. The imaginary part of admittance of the one-port structure, schematically depicted in Fig. 4.10, features the synchronous resonance at the left edge of reflector SB and the hiccup resonance in the middle of the SB. If the antiresonance frequency of the synchronous resonance coincides with the hiccup resonance frequency, the synchronous resonance acts as a matching inductance, in effect canceling the static capacitance of the hiccup resonance. Since the hiccup resonance is mainly responsible for the energy transfer from input to output and, therefore, for the filter PB, the matching significantly affects the shape of the PB, as can be seen from the experimental curves shown in Fig. 4.11 for a 2-IDT filter such as depicted in Fig. 4.9(a). Varying the period of the gap IDTs by $\pm 0.5\%$ shifts the hiccup resonance which creates the PB while the synchronous resonance remains practically unchanged. As the matching improves, the PB becomes more symmetric and IL reduces.

To observe self-matching, the lengths of the long IDTs and the dimensions of the distributed gap region need to be adjusted such that the resonance and anti-resonance frequencies coincide. In addition to this, the coupling coefficient, K^2, determining the

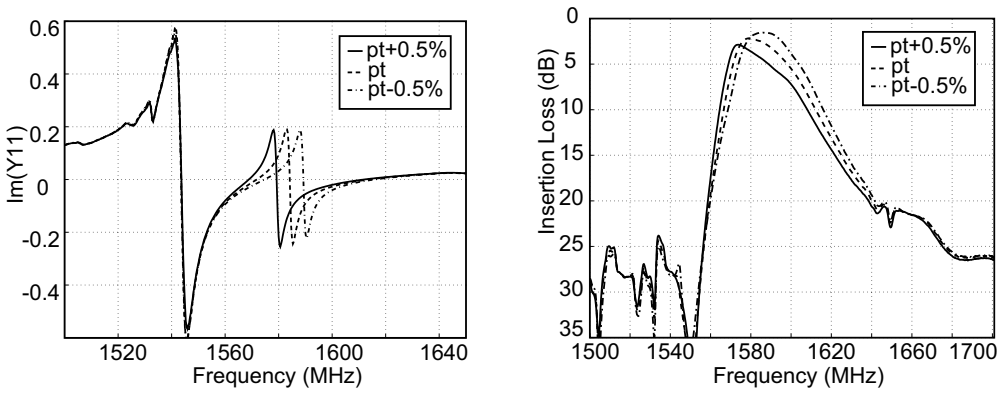

(a) (b)

Figure 4.11: Measured results illustrating the effect of the self-matching on the PB of a 2-IDT DRF. (a) As the period of the distributed gap is varied by 0.5%, the matching of the hiccup resonance changes. (b) The PB of a DRF, created by the hiccup resonance, improves as the self-matching improves.

anti-resonance frequency of the long IDTs and the reflection coefficient, κ, determining the width of the reflector SB, must be appropriately related for the matching condition to be met. If the hiccup resonance takes place in the middle of the grating SB (at the Bragg frequency of the reflector), the half-width of the SB relative to the Bragg frequency, determined by

$$\frac{\Delta f}{f_0} = \frac{|\kappa|}{2\pi}, \tag{4.1}$$

must be equal to the resonance-anti-resonance distance of the synchronous resonance, which in approximation is

$$\frac{f_{\mathrm{ar}} - f_0}{f_0} \approx \frac{K^2}{2}. \tag{4.2}$$

Therefore, we must have approximately

$$K^2 \approx \kappa/\pi. \tag{4.3}$$

A relatively strong piezoelectric substrate is required for the self-matching to be observed. For example for quartz, with $K^2 \approx 0.001$ and $\kappa \approx 0.04$, there is an order of magnitude difference and the self-matching condition will not be satisfied. On the other hand, for 42°-$LiTaO_3$ with $K^2 \approx 0.05$ and $\kappa \approx 0.2$, the condition can be met. If the hiccup resonance frequency is shifted away from the center of the reflector SB, the relation (4.3) will be modified.

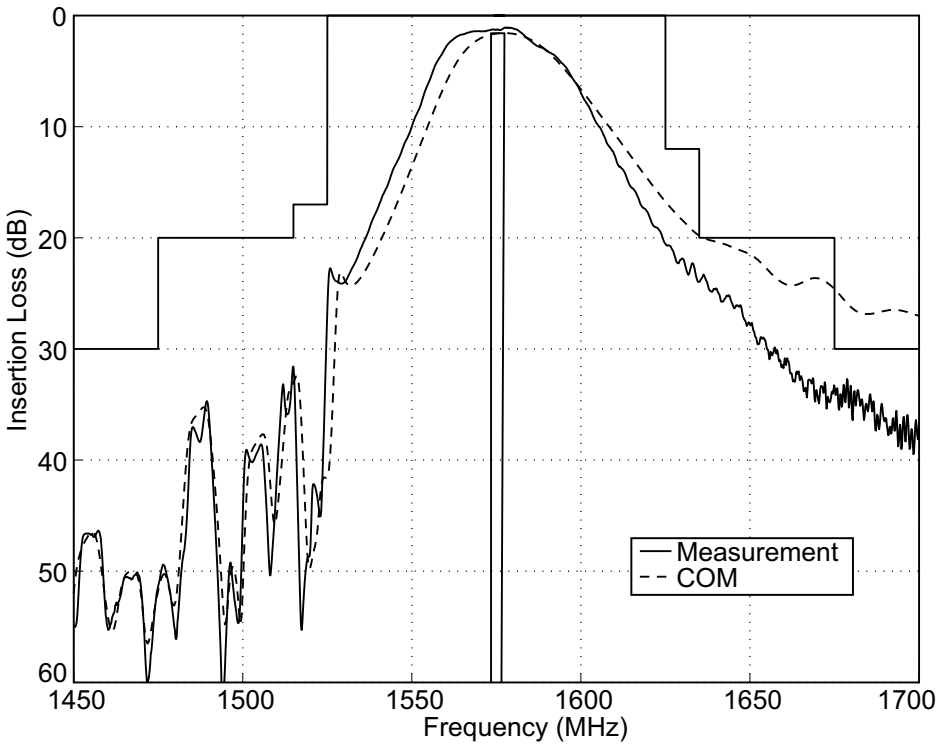

Figure 4.12: Measured frequency response of a balanced-output, 3-IDT DRF (solid line), with COM simulation (dashed line). The minimum IL in the PB is 1.07 dB, with an absolute 3-dB BW of 29 MHz (1.9%).

4.3.3 Experimental Results

A DRF having 3 IDTs, with an unbalanced input and a balanced output, consisting of two parallel-connected 3-IDT tracks with identical device parameters but inverted output polarities for BALUN functionality, was realized at 1575 MHz. The measured frequency response is depicted in Fig. 4.12 along with the corresponding COM simulation. The measured balance characteristics are shown in Fig. 4.13. The filter features an absolute 3-dB BW of 29 MHz (1.9%) with a minimum IL of 1.07 dB and suppression levels of 40 dB. The parallel-connected topology yields extremely flat phase characteristics, as depicted in Fig. 4.13(b). The amplitude imbalance in the PB (Fig. 4.13(a)) ranges from 0 dB to 2.1 dB, and the phase imbalance (Fig. 4.13(b)) from 1° to 4.5°. The specification lines plotted in Figs. 4.12 and 4.13 are for a low-loss GPS filter.

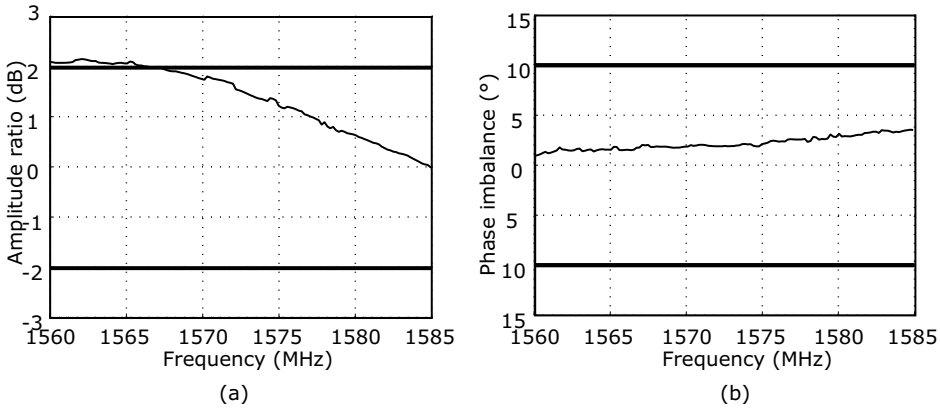

Figure 4.13: Measured balance characteristics of the 3-IDT DRF: amplitude (a) and phase (b) imbalance in the filter PB.

4.3.4 Comments and Conclusions

The unconventional configuration of the CRF studied here was earlier referred to as "degenerated CRF" [181]. This work enhanced the understanding of the operation of the structure and explained why earlier experiments featured high losses. The self-matching phenomenon described here allows to use the inductive admittance of the synchronous resonance to cancel the static capacitance of the hiccup resonance, enabling low-loss devices based on the the hiccup resonance of the structure. A novel type of low-loss filter based on this phenomenon, yielding 1%–2% relative bandwidth, was introduced, and prototype devices for the GPS specification yield excellent low-loss performance.

5 Related Results and Observations

This Chapter summarizes auxiliary results obtained in the course of this work. The features of non-synchronous resonators on LSAW substrates, published in Paper VI, are discussed in 5.1. The effect of stray capacitances due to contact pads on filter performance is demonstrated in 5.2.

5.1 Non-Synchronous Resonators on a Leaky-Wave Substrate

Conventionally, SAW resonators have been studied on quartz for maximized temperature stability. Synchronous resonators, having the same period in reflectors and in IDTs, as well as hiccup-type resonators, have good manufacturability because the center frequency is virtually independent of the reflectivity of the electrodes [5]. However, non-synchronous resonators can have better Q-factors than synchronous resonators [183].

On substrates with high K^2 and thick electrodes, hiccup-type gaps in synchronous structures are avoided because of the high reflectivity of the electrodes. The resonance is shifted to the left edge of the reflector SB and SAW amplitude at the resonance frequency is close to uniform over the IDT. This provides high coupling (resonance-antiresonance frequency separation) necessary to obtain a wide PB in, e.g., ladder filters [12]. Nevertheless, in synchronous resonators on high-K^2 substrates the reflectivity of the reflector gratings is not optimal at the resonance frequency. Consequently, a significant fraction of the acoustic energy is distributed inside the reflectors, and the strength of the resonance is reduced. Furthermore, the shape of the resonance can be compromised and the Q-factor reduced.

In the research reported in [VI], structures having resonance in the center of reflector SB were studied to obtain improved performance on LSAW substrates. The DR resonator discussed in Section 4.3 exhibits hiccup-type resonant behaviour on LSAW substrates, with the hiccup resonance situated in the center of the reflector SB. Self-matching the hiccup resonance with the synchronous resonance and replacing open-surface gaps with their distributed counterparts are essential for the operation of the device.

We also investigated non-synchronous resonators having different period in reflectors and IDTs. In such a structure, the resonance can be shifted to the center of the reflector SB, as illustrated in Fig. 5.1. This yields improved performance in terms of both resonance shape and strength. Simulated distributions of the acoustic amplitude in a non-synchronous and a corresponding synchronous resonators are shown in Fig. 5.2. The amplitude distributions confirm that at the resonance frequency, the acoustic en-

Table I: Device parameters for synchronous and non-synchronous resonator structures studied in this work.

Parameter	Synchronous	Non-synchronous
Aperture (μm)	146	146
Number of fingers in reflectors	69	69
Number of fingers in IDT	45	45
Period in reflectors (μm)	1.02	1.02
Period in IDT (μm)	1.02	0.976

ergy is more effectively confined inside the IDT region in the non-synchronous resonator. Parameters for both synchronous and non-synchronous resonators are summarized in Table I.

At the resonance frequency $f_0 = 2003$ MHz, an experimental resonance-anti-resonance distance of 44 MHz and a Q-value of 582 were achieved for a non-synchronous resonator.

The drawback of such a structure, considering its application in ladder filters, is that the anti-resonance frequency can be shifted outside the reflector SB. This may create undesired ripple in the ladder filter PB. Moreover, the BAW radiation region of the reflectors, beginning at frequencies slightly higher than the antiresonance frequency, might interfere with the filter PB. Therefore, non-synchronous resonators probably will not be optimal for ladder filter applications, at least not as parallel elements. They can, however, find applications as parallel resonator for CRFs, improving rejection or creating a notch above the filter PB in order to suppress the characteristic CRF sidelobe.

5.2 Effect of Contact Pad Capacitances

In a SAW filter, elements such as metallized contact pads, bond wires, and package have to be considered as parasitic elements connected to the filter. At 2-GHz range the package capacitances can be comparable to the static capacitance of an IDT. In this section, the contact pad capacitances connecting input and output of the filter and their effect on the filter performance is discussed from an experimental point of view [II].

A simple example of a contact pad layout for a 3-IDT CRF is illustrated in Fig. 5.3. Parasitic capacitances due to the contacts arise between the input and output ports, i.e., C_1 between the input and the output 1, and C_2 between the input and the output 2. Filter performance is determined not only by the acoustic signals processed in the

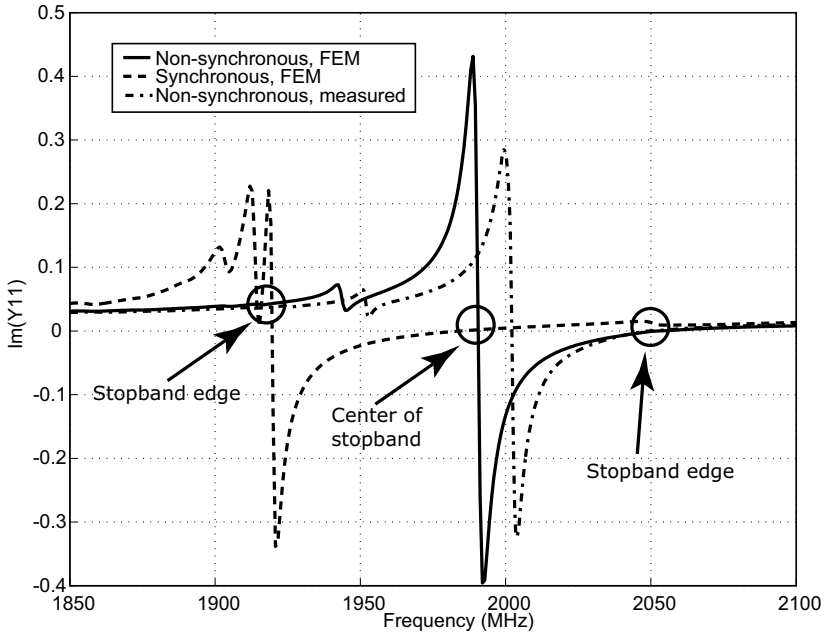

Figure 5.1: Simulated and experimental admittance (imaginary part) of a non-synchronous resonator (solid and dash-dotted lines) and a synchronous resonator (dashed line). In the synchronous resonator, the resonance is situated at the left edge of the reflector SB. In a non-synchronous resonator, the resonance is shifted to the center of the SB.

filter structure but also by EM signals passing through C_1 and C_2.

The size of one side of input and output contact pads is typically 100–200 μm. The resulting capacitance between the input and the output is on the order of 10 fF. This capacitance can lead to the direct coupling of the signal from the input to the output, which decreases the suppression levels outside the PB of the filter. Other effects of the coupling capacitances are the distortion of the shape of the PB and the deterioration of the balance between balanced outputs.

The direct coupling of EM signal can be significantly reduced, if the filter operates in a balanced-output mode. In such a case, if the output contact pads are identical with respect to the input such that the signals passing through C_1 and C_2 are equal, their contribution to the differential signal is cancelled. Experimental observation of this effect is presented in Fig. 5.4, which shows the frequency responses of a 3-IDT balanced filter (solid line) and a corresponding 2-IDT single-ended filter (dashed line). A considerable increase in the suppression levels can be observed in the balanced device. Nevertheless, EM coupling in the common mode is still present, leading to deterioration of the balance between the output signals.

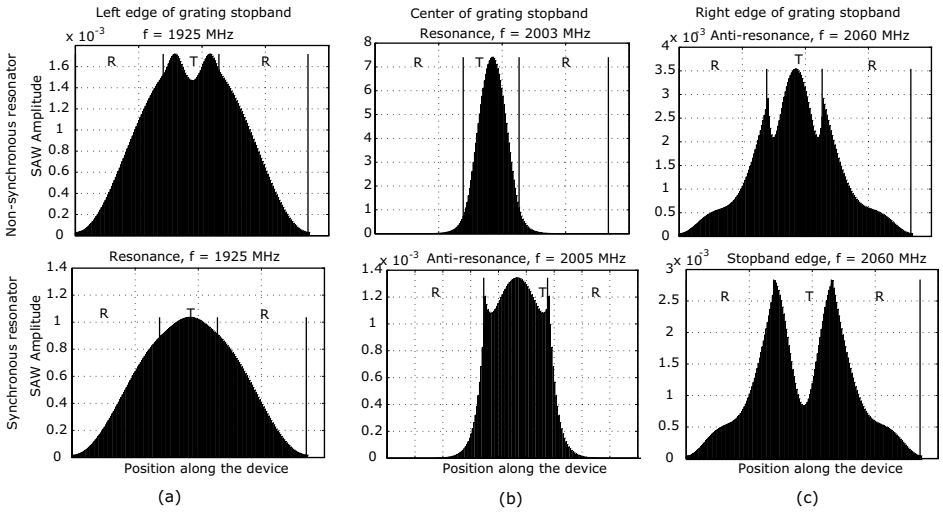

Figure 5.2: Simulated (COM) SAW amplitude distributions for a non-synchronous (above) and a synchronous (below) resonator. Boundaries of the acoustical elements (R–reflector, T–transducer) are shown with vertical lines. At the resonance frequency of the synchronous resonator (a), a significant amount of acoustic energy is inside the reflectors, whereas for a non-synchronous resonator (b), it is efficiently confined into the IDT.

To minimize the parasitic capacitances, the distance between the input and output pads can be increased. To study this effect, two pad layouts depicted in Fig. 5.5 were realized. In layout 1, the input and output pads are located on opposite sides of the filter track, whereas in layout 2, the pads are situated on the same side. Figs. 5.6 and 5.7 show the measured response of a balanced-output CRF with 5 IDTs for the two contact pad topologies. A small difference in the IL and rejections is seen in Fig. 5.6, but the effect on the amplitude and phase balance (Fig. 5.7) is more pronounced. Separating the pads yields a more slow-varying response with smaller deviation from the balanced state. It should, however, be noted that the contact pad topology is not the only factor affecting the response. Changed ground connections between the two layouts in Fig. 5.5 can also contribute to the frequency response. The balance is further affected by the capacitances between electrodes at the interface of adjacent IDTs.

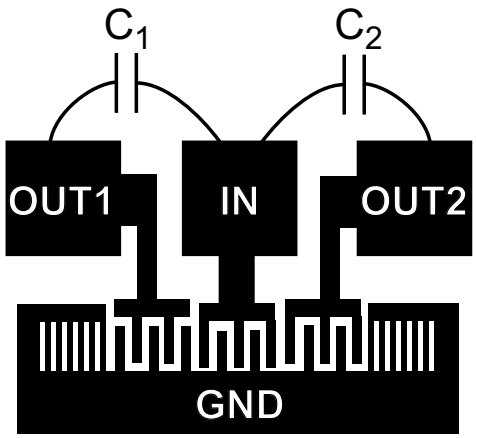

Figure 5.3: Example of a contact pad topology for a 3-IDT CRF.

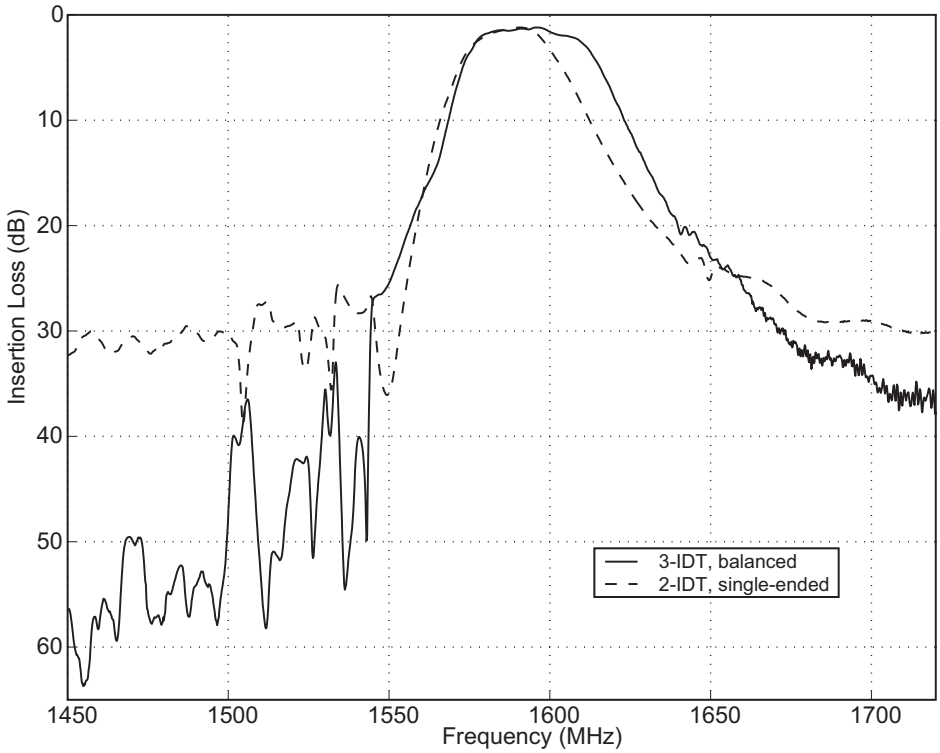

Figure 5.4: Experimental frequency response of a balanced-output 3-IDT CRF (solid line) and a corresponding single-ended 2-IDT CRF (dashed line). Due to the direct coupling capacitances, the rejection of the signal in the 2-IDT device is reduced.

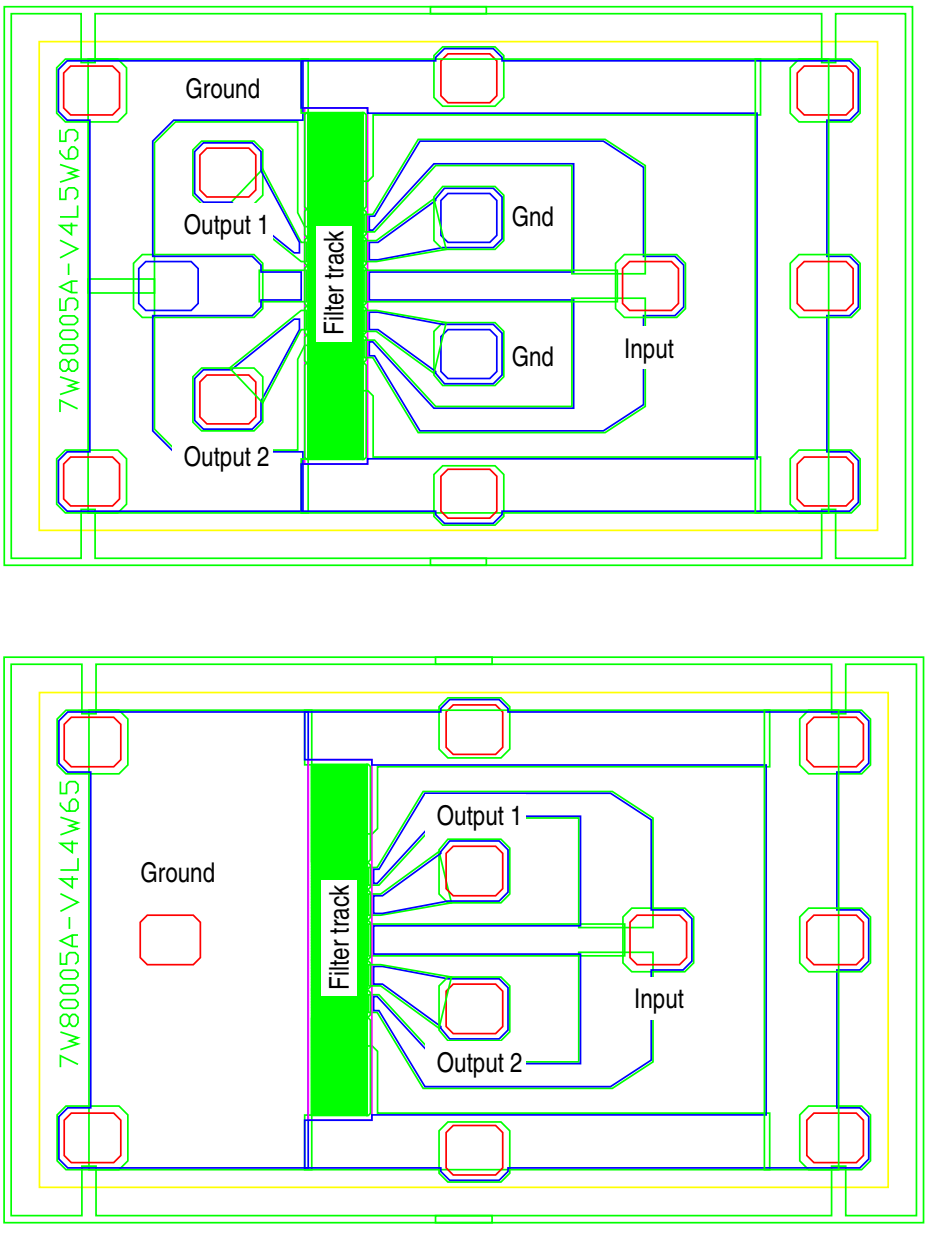

Figure 5.5: Mask layouts for 2 contact pad topologies for a balanced-output 5-IDT CRF. *Above:* Input and output contact pads are separated (layout1). *Below:* Input and output pads are situated on the same side of the filter track (layout 2).

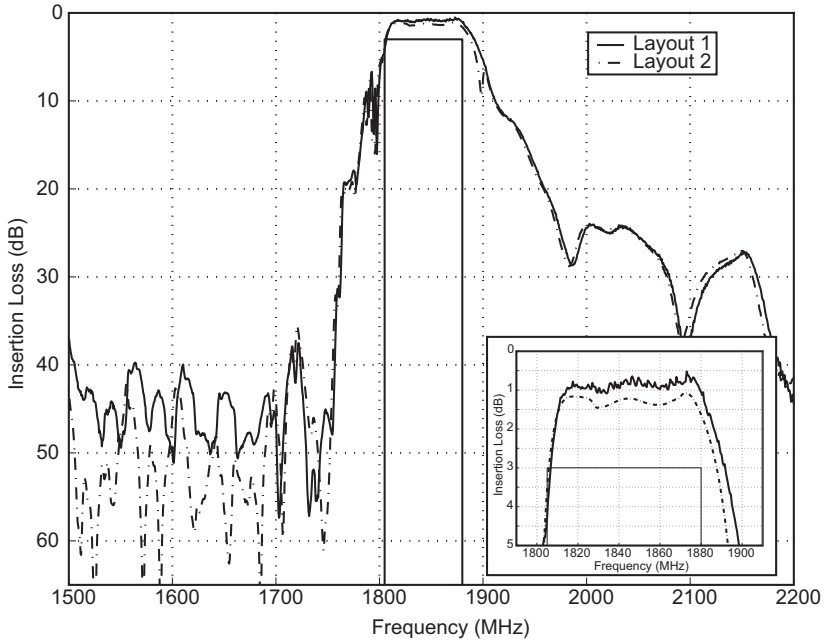

Figure 5.6: Measured frequency response of a balanced-output CRF for two contact pad topologies. In layout 1 (solid line), the input and output pads are placed on opposite sides of the filter track, whereas in layout 2 (dashed line) they are on the same side.

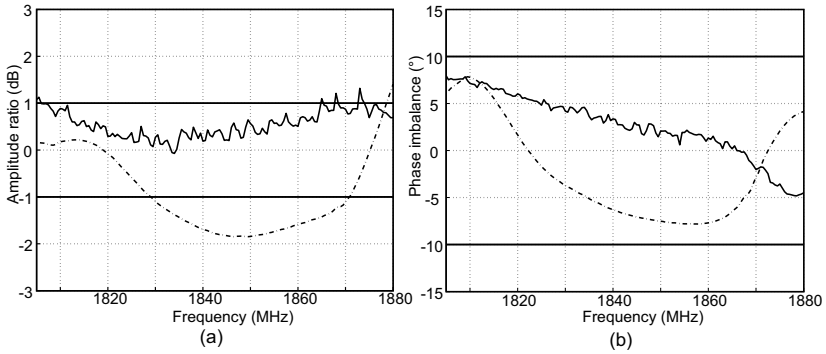

Figure 5.7: Effect of the contact pad layout on the measured balance characteristics of a 5-IDT CRF: amplitude (a) and phase (b) imbalance in the PB for layout 1 (solid line) and layout 2 (dashed line).

6 Discussion

The work presented in this thesis focuses on loss mechanisms in LSAW coupled resonator filters and on methods for suppressing said mechanisms in order to obtain improved device performance at 1–2 GHz frequencies. The main accomplishments of this research comprise the design and analysis of several filter topologies that reduce resistive losses and losses resulting from BAW back-scattering of LSAW. An important result is the novel double-resonance filter presented and analyzed in this work.

Within this research work, a simulation and optimization tool for coupled SAW filters was developed. The optimization tool enables a straightforward cascading of multiple acoustical elements, such as IDTs and reflectors, facilitating fast and efficient design of multi-element CRFs, and specifically, distributed-gap devices. Although the simulation is based on the COM model, leaky-wave characteristics are incorporated into the model as empirical parameters. In order to improve the optimization process, stochastic optimization algorithms, designed to search for the global extrema of the objective function and specifically suited for multi-element CRFs, were developed and implemented.

The connective design concept for the filter structures presented in this thesis is the use of the distributed-gap structure to reduce propagation and bulk-wave conversion loss. Furthermore, all of the designs strive for reducing the resistive losses of the CRF structure by decreasing the aperture and increasing the number of electrodes in the IDTs.

The novel structures described for the first time in this research comprise (i) a filter with two different CRF tracks operating in parallel, (ii) a 5-IDT CRF with distributed gaps having extremely low IL (< 1 dB) at 1.8 GHz, and (iii) a novel double-resonance structure and filters based on that, designed for operation at 1.6 GHz (GPS range) and exhibiting low IL on the order of 1 dB. The operation of the proposed structures is discussed in detail, giving due consideration to the effect of the device parameters on the response of the structures. The DRF structure is described and its operation is analyzed, and the predicted operation principle is confirmed by experimental results obtained with laser-interferometric measurements.

Compared with concurrent work as reported in publications [90, 109–112, 121], the CRF designs discussed in this thesis show comparable or improved performance. The reported IL level at 1.8 GHz and 1.9 GHz is around 1.5 dB [90, 110, 112]. In this work, IL smaller than 1.0 dB with ripple less than 0.5 dB was achieved at 1842 MHz. The improvement in the loss level is considerable.

In the same frequency range, improved balance characteristics of ± 0.5 dB for am-

plitude imbalance and $\pm 4^\circ$ and $-2^\circ/+3^\circ$ for phase imbalance are reported [90, 109]. At 1.8 GHz, the 5-IDT filter described here has $0 \ldots 1$ dB amplitude imbalance and -5°/+8° phase imbalance, giving only slightly inferior performance even though balance characteristics were not the focus in the design process. The layout of contact pads was shown to affect the balance characteristics considerably. At 1.6 GHz, the DRF structure with two tracks shows extremely flat phase characteristics with measured phase imbalance in the filter PB ranging from 1° to 4.5°.

Both the 5-IDT approach and the parallel-track design studied in this thesis work aim for very wide-band, low-loss performance, and both are capable of balanced operation. The parallel-track filter yields improved rejection especially immediately above PB. On the other hand, as discussed in Section 4.1, it is rather sensitive to design and fabrication parameters in terms of both PB and suppression levels. The 5-IDT filter with distributed gaps promises lower IL in the PB and a more robust design, but does not have as steep transition above the PB.

The results obtained in this research work indicate that distributed gaps are essential for achieving extremely low-loss performance at GHz frequencies, leading to the need of fast and accurate simulation of cascades of multiple acoustical elements. The COM model is, in principle, the ideal tool for CRF optimization, as it offers relatively simple analytical formulas that describe the acoustical operation of the devices. For short IDT sections such as distributed gaps, however, the limitations of the COM model become apparent, as the structures become so short that the validity of the model is compromised. In that case, effects such as stray capacitances between adjacent IDTs should be accounted for in the simulations. In order to develop a powerful and reliable simulation and optimization tool, a way should be found to incorporate these effects into the model while retaining the flexibility and speed of the COM model combined with the transmission matrix scheme.

Improving the performance of CRFs is a topical issue, with new results continuously introduced by the research community. Recently, CRFs with an increased number of degrees of freedom in the design have been proposed [112,129]. They use modulation of the IDT period to achieve improved performance. In principle, the approach is similar to the distributed-gap approach implemented in this research, but the concept is taken one step further by increasing the number of reduced-period elements. Applying such a topology further increases the number of cascaded elements, stressing the need for an efficient simulation and optimization tool. Moreover, as the length of the individual elements is further reduced, models taking into account effects arising from finite element length are required.

The research described in this thesis has resulted in considerable reduction in the

insertion loss of coupled SAW filters, as well as in an original resonator filter structure for low-loss, narrow-band operation on LSAW substrates. Further improvement in CRF performance is possible, and reducing the IL to less than 1 dB and improving the balance performance are perhaps the most important goals at the moment. Research summarized in this thesis shows that considerable reduction in the IL is achievable if important loss mechanisms are taken into account and their effect is minimized with proper design. Improving balance characteristics requires both novel filter designs, optimized contact pad topologies and more accurate simulation tools. In investigating novel filter topologies and design approaches, global optimization can be a powerful tool, as it facilitates the designer's task in a situation with no known good starting point for optimization.

Coupled resonator filter is one of the most popular design approaches in modern low-loss SAW filters. To hold that place in the face of increasing competition from other technologies, constant performance improvements are necessary. This work summarizes some such improvements. A lot remains to be done, though, and the field of coupled SAW filters remains an active one, as well as attractive for future research.

References

[1] C. K. Campbell, *Surface Acoustic Wave Devices for Mobile and Wireless Communications*. San Diego: Academic Press, Inc., 1998.

[2] K. Hashimoto, *Surface Acoustic Wave Devices in Telecommunications: Modelling and Simulation*. Berlin: Springer-Verlag, 2000.

[3] D. P. Morgan, *Surface-Wave Devices for Signal Processing*. Amsterdam: Elsevier, 1991.

[4] B. R. Potter and C. S. Hartmann, "Low loss surface-acoustic-wave filters", *IEEE Trans. Parts, Hybrids, Packag.* **13**, pp. 348–353 (1977).

[5] P. V. Wright, "A review of SAW resonator filter technology", in *Proc. 1992 IEEE Ultrasonics Symposium*, pp. 29–38 (1992).

[6] M. Solal and J.-M. Hode, "A new compact SAW low loss filter for mobile radio", in *Proc. of the 1993 IEEE Ultrasonics Symposium*, pp. 105–109 (1993).

[7] Y. Yamamoto, "SAW filters and resonators for public communication systems", in *Proc. of the 1993 Ultrasonics Symposium*, pp. 95–103 (1993).

[8] D. P. Morgan and T. Thorvaldsson, "A new low-loss SAW filter technique", in *Proc. of the 1994 IEEE Ultrasonics Symposium*, pp. 23–26 (1994).

[9] M. A. Sharif, C. Lambert, D. P. Chen, and C. S. Hartmann, "Network coupled, high performance SAW resonator filters", in *Proc. of the 1994 IEEE Ultrasonics Symposium*, pp. 135–138 (1994).

[10] T. Thorvaldsson, V. P. Plessky, S. Muckenhirn, and M. Joray, "GHz range STW resonators and narrow band filters", in *Proc. of the 1994 IEEE Ultrasonics Symposium*, pp. 99–102 (1994).

[11] K. M. Lakin, G. R. Kline, and K. T. McCarron, "Development of miniature filters for wireless applications", *IEEE Trans. Microwave Theory Tech.* **43**, pp. 2933–2939 (1995).

[12] V. P. Plessky, "SAW impedance elements", *IEEE Trans. Ultrason., Ferroelect., Freq. Contr.* **42**, pp. 870–875 (1995).

[13] M. Kadota, T. Yoneda, K. Fujimoto, T. Nakao, and E. Takata, "Very small-sized resonator filter using shear horizontal wave on quartz", *Jpn. J. Appl. Phys.* **40**, pp. 3718–3721 (2001).

[14] R. Weigel, D. P. Morgan, J. M. Owens, A. Ballato, K. M. Lakin, K. Hashimoto, and C. C. W. Ruppel, "Microwave acoustic materials, devices, and applications", *IEEE Trans. Microwave Theory Tech.* **50**, pp. 738–749 (2002).

[15] I.-T. Tang, F.-L. Jenq, J.-H. Horng, M.-P. Houng, and Y.-H. Wang, "A novel microwave microstrip surface acoustic wave filter with gigahertz band low-loss wide bandwidth for broad spectrum communication system", *Jpn. J. Appl. Phys.* **41**, pp. 2974–2977 (2002).

[16] S. V. Kiselev, E. I. Fedorov, and V. S. Orlov, "SAW filters with combined single-mode and double-mode sections", in *Proc. of the 2002 IEEE Ultrasonics Symposium*, pp. 179–183 (2002).

[17] T. Shiba, M. Ide, and Y. Fujita, "Miniaturized SAW filter using unidirectional quadrature IDT couplers", in *Proc. of the 2003 IEEE Ultrasonics Symposium*, pp. 2093–2096 (2003).

[18] F. Schmidt, O. Sczesny, L. Reindl, and V. Mágori, "Remote sensing of physical parameters by means of passive surface acoustic wave devices ("ID-TAG")", in *Proc. of the 1994 IEEE Ultrasonics Symposium*, pp. 589–592 (1994).

[19] V. P. Plessky, S. N. Kondratiev, and F. Stierlin, R. Nyffeler, "SAW tags: New ideas", in *Proc. of the 1995 IEEE Ultrasonics Symposium*, pp. 117–120 (1995).

[20] C. S. Hartmann, "A global SAW ID tag with large data capacity", in *Proc. of the 2002 IEEE Ultrasonics Symposium*, pp. 65–69 (2002).

[21] T. F. Bechteler and H. Yenigün, "2-D localization and identification based on SAW ID-tags at 2.5 GHz", *IEEE Trans. Microwave Theory Tech.* **51**, pp. 1584–1590 (2003).

[22] D. S. Ballantine, Jr., R. M. White, S. J. Martin, A. J. Ricco, E. T. Zellers, G. C. Frye, and H. Wohltjen, *Acoustic Wave Sensors: Theory, Design and Physico-Chemical Applications*, ser. Applications of Modern Acoustics. San Diego: Academic Press, 1997.

[23] M. Thompson and D. C. Stone, *Surface-Launched Acoustic Wave Sensors: Chemical Sensing and Thin-Film Characterization*, ser. Chemical Analysis. New York: John Wiley & Sons, Inc., 1997.

[24] Lord Rayleigh, "On waves propagated along the plane surface of an elastic solid", *Proc. London Math. Society* **17**, pp. 4–11 (1885).

[25] J. Curie and P. Curie, "Développement par pression, de l'électricité polaire dans les cristaux hémièdres à faces inclinées", *Comptes Rendus* **91**, p. 294 (1880).

[26] W. G. Cady, *Piezoelectricity.* New York: McGraw-Hill, 1946.

[27] T. Ikeda, *Fundamentals of Piezoelectricity.* Oxford: Oxford University Press, 1996.

[28] H. F. Tiersten, *Linear Piezoelectirc Plate Vibrations.* New York: Plenum Press, 1969.

[29] R. M. White and F. W. Voltmer, "Direct piezoelectric coupling to surface elastic waves", *Appl. Phys. Lett.* **7**, pp. 314–316 (1965).

[30] K. Bløtekjær, K. A. Ingebrigtsen, and H. Skeie, "A method for analyzing waves in structures consisting of metal strips on dispersive media", *IEEE Trans. Electron Devices* **20**, pp. 1133–1138 (1973).

[31] K. Bløtekjær, K. A. Ingebrigtsen, and H. Skeie, "Acoustic surface waves in piezoelectric materials with periodic metal strips on the surface", *IEEE Trans. Electron Devices* **20**, pp. 1139–1146 (1973).

[32] H. A. Haus and R. V. Schmidt, "Transmission response of cascaded gratings", *IEEE Trans. Sonics Ultrason.* **24**, pp. 94–101 (1977).

[33] H. A. Haus, "Modes in SAW grating resonators", *J. Appl. Phys.* **48**, pp. 4955–4961 (1977).

[34] H. A. Haus and K. L. Wang, "Modes of grating waveguide", *J. Appl. Phys.* **49**, pp. 1061–1069 (1978).

[35] D.-P. Chen and H. A. Haus, "Analysis of metal-strip SAW gratings and transducers", *IEEE Trans. Sonics Ultrason.* **32**, pp. 395–408 (1985).

[36] H. Bachl, G. Kovacs, K. C. Wagner, and A. R. Baghai-Wadji, "Accurate and fast two-dimensional analysis of long, apodized SAW-transducers", in *Proc. of the 1990 Ultrasonics Symposium*, pp. 417–420 (1990).

[37] D. P. Morgan, "Admittance calculations for non-reflective SAW transducers", in *Proc. of the 1996 IEEE Ultrasonics Symposium*, pp. 131–134 (1996).

[38] E. A. Ash and E. G. S. Paige, Eds., *Rayleigh-Wave Theory and Application*. Berlin: Springer-Verlag, 1985.

[39] B. A. Auld, *Acoustic Fields and Waves in Solids*. New York: John Wiley & Sons, 1973.

[40] K. Hashimoto, G. Q. Zheng, and M. Yamaguchi, "Fast analysis of SAW propagation under multi-electrode-type gratings with finite thickness", in *Proc. of the 1997 IEEE Ultrasonics Symposium*, pp. 279–284 (1997).

[41] C. Elachi, "Waves in active and passive periodic structures: A review", *Proc. IEEE* **64**, pp. 1666–1698 (1976).

[42] R. T. Smith, "Elastic, piezoelectric, and dielectric properties of lithium tantalate", *Appl. Phys. Lett.* **11**, pp. 146–148 (1967).

[43] K. Nakamura, M. Kazumi, and H. Shimizu, "SH-type and Rayleigh-type surface waves on rotated Y-cut $LiTaO_3$", in *Proc. of the 1977 Ultrasonics Symposium*, pp. 819–822 (1977).

[44] C. S. Hartmann, V. P. Plessky, and S. Jen, "112°-$LiTaO_3$ periodic waveguides", in *Proc. of the 1995 IEEE Ultrasonics Symposium*, pp. 63–66 (1995).

[45] O. Kawachi, G. Endoh, M. Ueda, O. Ikata, K. Hashimoto, and M. Yamaguchi, "Optimum cut of $LiTaO_3$ for high performance leaky surface acoustic wave filters", in *Proc. of the 1996 IEEE Ultrasonics Symposium*, pp. 71–76 (1996).

[46] K. Hashimoto, M. Yamaguchi, S. Mineyoshi, O. Kawachi, M. Ueda, and G. Endoh, "Optimum leaky-SAW cut of $LiTaO_3$ for minimised insertion loss devices", in *Proc. of the 1997 IEEE Ultrasonics Symposium*, pp. 245–254 (1997).

[47] O. Kawachi, S. Mineyoshi, G. Endoh, M. Ueda, O. Ikata, K. Hashimoto, and M. Yamaguchi, "Optimal cut for leaky SAW on $LiTaO_3$ for high performance resonators and filters", *IEEE Trans. Ultrason., Ferroelect., Freq. Contr.* **48**, pp. 1442–1448 (2001).

[48] N. Naumenko and B. Abbott, "Optimized cut of $LiTaO_3$ for resonator filters with improved performance", in *Proc. of the IEEE Ultrasonics Symposium*, pp. 385 – 390 (2002).

[49] G. Kovacs, M. Anhorn, H. E. Engan, G. Visintini, and C. C. W. Ruppel, "Improved material constants for $LiNbO_3$ and $LiTaO_3$", in *Proc. of the 1990 Ultrasonics Symposium*, pp. 435–438 (1990).

[50] C. S. Hartmann and V. P. Plessky, "Experimental measurements of propagation, attenuation, reflection and scattering of leaky waves in Al electrode gratings on 41°, 52° and 64°-$LiNbO_3$", in *Proc. of the 1993 Ultrasonics Symposium*, pp. 1247–1250 (1993).

[51] K. Yamanouchi, G. Shimizu, and K. Morishita, "2.5-GHz-range SAW propagation and reflection characteristics and application to passive electronig tag and matched filter", in *Proc. of the 1993 IEEE Ultrasonics Symposium*, pp. 1267–1270 (1993).

[52] J. Kushibiki, I. Takanaga, M. Arakawa, and T. Sannomiya, "Accurate measurements of the acoustical physical constants of $LiNbO_3$ and $LiTaO_3$ single crystals", *IEEE Trans. Ultrason., Ferroelect., Freq. Contr.* **46**, pp. 1315–1323 (1999).

[53] T. Sato and H. Abe, "Propagation of longitudinal leaky surface waves under periodic metal grating structure on lithium tetraborate", *IEEE Trans. Ultrason., Ferroelect., Freq. Contr.* **45**, pp. 394–408 (1998).

[54] A. Bungo, C. Jian, K. Yamaguchi, Y. Sawada, S. Uda, and Y. P. Pisarevsky, "Analysis of surface acoustic wave properties of the rotated Y-cut langasite substrate", *Jpn. J. Appl. Phys.* **38**, pp. 3239–3243 (1999).

[55] M. Kadota, J. Nakanishi, T. Kitamura, and M. Kumatoriya, "Surface acoustic wave properties on rotated Y-cut langasite single crystal substrates", in *Proc. of the 1998 IEEE International Symposium on Applications of Ferroelectrics*, pp. 357–360 (1998).

[56] S. N. Kondratiev, T. Thorvaldsson, S. A. Sakharov, O. A. Buzanov, and A. V. Medvedev, "Extraction of COM parameters on langasite substrates and the application to design of SAW filter", in *Proc. of the 2001 IEEE Ultrasonics Symposium*, pp. 53–56 (2001).

[57] S. Lehtonen, V. P. Plessky, C. S. Hartmann, and M. M. Salomaa, "Extraction of the SAW attenuation parameter in periodic reflecting grating", *IEEE Trans. Ultrason., Ferroelect., Freq. Contr.* **52**, pp. 111–119 (2005).

[58] Y. Zhang, J. Desbois, and L. Boyer, "Characteristic parameters of surface acoustic waves in a periodic metal grating on a piezoelectric substrate", *IEEE Trans. Ultrason., Ferroelect., Freq. Contr.* **40**, pp. 183–192 (1993).

[59] J. Koskela, V. P. Plessky, and M. M. Salomaa, "SAW/LSAW COM parameter extraction from computer experiments with harmonic admittance of a periodic array of electrodes", *IEEE Trans. Ultrason., Ferroelect., Freq. Contr.* **46**, pp. 806–816 (1999).

[60] H. Engan, K. A. Ingebrigtsen, and A. Tonning, "Elastic surface waves in α-quartz: Observation of leaky surface waves", *Appl. Phys. Lett.* **10**, pp. 311–313 (1967).

[61] H. Meier and P. Russer, "Analysis of leaky surface acoustic waves on $LiTaO_3$ substrate", in *Proc. of the 1992 Annual Frequency Control Symposium*, pp. 378–383 (1992).

[62] V. P. Plessky and C. S. Hartmann, "Characteristics of leaky SAWs on 36-$LiTaO_3$ in periodic structures of heavy electrodes", in *Proc. of the 1993 IEEE Ultrasonics Symposium*, pp. 1239–1242 (1993).

[63] S. Tonami, A. Nishikata, and Y. Shimizu, "Characteristics of leaky surface acoustic waves propagating on $LiNbO_3$ and $LiTaO_3$ substrates", *Jpn. J. Appl. Phys.* **34**, pp. 2664–2667 (1995).

[64] U. Rösler, D. Cohrs, A. Dietz, G. Fischerauer, W. Ruile, P. Russer, and R. Weigel, "Determination of leaky SAW propagation, reflection and coupling on $LiTaO_3$", in *Proc. of the 1995 IEEE Ultrasonics Symposium*, pp. 247–250 (1995).

[65] V. I. Grigorievski, "Interaction between leaky surface acoustic waves in periodic gratings of thick metal electrodes", in *Proc. of the 2002 IEEE Ultrasonics Symposium*, pp. 339–342 (2002).

[66] N. E. Glass and A. A. Maradudin, "Leaky surface-elastic waves on both flat and strongly corrugated surfaces for isotropic, nondissipative media", *J. Appl. Phys.* **54**, pp. 796–805 (1983).

[67] C. K. Campbell, "Longitudinal-mode leaky SAW resonator filters on 64° Y-X lithium niobate", *IEEE Trans. Ultrason., Ferroelect., Freq. Contr.* **42**, pp. 883–888 (1995).

[68] Y. Kobayashi, Y. Hirao, K. Takeuchi, T. Usuki, K. Shibata, and Y. Shimizu, "New high-phase-velocity surface acoustic wave mode on $LiTaO_3$ and $LiNbO_3$", *Jpn. J. Appl. Phys.* **34**, pp. L1309–L1310 (1995).

[69] T. Sato and H. Abe, "Longitudinal leaky surface waves for high frequency SAW device applications", in *Proc. of the 1995 IEEE Ultrasonics Symposium*, pp. 305–315 (1995).

[70] Y. Kobayashi, N. Tanaka, K. Matsui, H. Okano, T. Usuki, K. Shibata, and Y. Shimizu, "1.9-GHz-band surface acoustic wave device using second leaky wave on $LiTaO_3$ and $LiNbO_3$", in *Proc. of the 1996 Annual IEEE International Frequency Control Symposium*, pp. 240–247 (1996).

[71] T. Sato and H. Abe, "Propagation properties of longitudinal leaky surface waves on lithium tetraborate", *IEEE Trans. Ultrason., Ferroelect., Freq. Contr.* **45**, pp. 136–151 (1998).

[72] T. Sato and H. Abe, "SAW device applications of longitudinal leaky surface waves on lithium tetraborate", *IEEE Trans. Ultrason., Ferroelect., Freq. Contr.* **45**, pp. 1506–1516 (1998).

[73] A. Isobe, M. Hikita, and K. Asai, "Propagation characteristics of longitudinal leaky SAW in Al-grating structures", *IEEE Trans. Ultrason., Ferroelect., Freq. Contr.* **46**, pp. 849–855 (1999).

[74] Y. V. Gulyaev and V. I. Grigorievski, "Reflection properties of fast leaky surface acoustic waves on lithium tetraborate", in *Proc. of the 1999 IEEE Ultrasonics Symposium*, pp. 185–188 (1999).

[75] V. I. Grigorievski, "Fast leaky surface acoustic waves on lithium niobate and lithium tantalate", in *Proc. of the 2000 IEEE Ultrasonics Symposium*, pp. 259–262 (2000).

[76] V. I. Grigorievski, "Resonant properties of fast leaky surface acoustic waves on lithium niobate", in *Proc. of the 2001 IEEE Ultrasonics Symposium*, pp. 197–199 (2001).

[77] T. Makkonen, V. P. Plessky, V. I. Grigorievski, L. Kopp, M. Solal, W. Steichen, and M. M. Salomaa, "FEM/BEM simulation and experimental study of LLSAW resonator characteristics on YZ-$LiNbO_3$", in *Proc. of the 2002 IEEE Ultrasonics Symposium*, pp. 317–320 (2002).

[78] T. Makkonen, V. P. Plessky, W. Steichen, and M. M. Salomaa, "Surface-acoustic-wave devices for the 2.5-5 GHz frequency range based on longitudinal leaky waves", *Appl. Phys. Lett.* **82**, pp. 3351–3353 (2003).

[79] Y. V. Gulyaev, V. I. Grigorievski, and V. P. Plessky, "Longitudinal leaky surface acoustic waves in periodic systems of metal electrodes on lithium niobate", in *Proc. of the 2003 IEEE Ultrasonics Symposium*, pp. 2118–2121 (2003).

[80] M. Kadota, E. Takata, M. Nakagawa, M. Tose, and Y. Yamamoto, "Low loss intermediate-frequency resonator filter using shear horizontal type leaky surface acoustic wave on α-phase heavy metal film/quartz", *Jpn. J. Appl. Phys.* **43**, pp. 3047–3049 (2004).

[81] T. Makkonen, V. P. Plessky, W. Steichen, V. I. Grigorievski, M. Solal, and M. M. Salomaa, "Longitudinal leaky SAW resonators and filters on YZ-$LiNbO_3$", *IEEE Trans. Ultrason., Ferroelect., Freq. Contr.* **53**, pp. 393–401 (2006).

[82] D. M. Pozar, *Microwave Engineering*. New York: John Wiley & Sons, 1998.

[83] J. F. Rosenbaum, *Bulk Acoustic Wave Theory and Devices*. Boston: Artech House, 1988.

[84] T. Morita, Y. Watanabe, M. Tanaka, and Y. Nakazawa, "Wideband low loss double mode SAW filters", in *Proc. 1992 IEEE Ultrasonics Symposium*, pp. 95–104 (1992).

[85] V. Plessky, "SAW devices for mobile communications", book manuscript.

[86] Y. Yamamoto and R. Kajihara, "SAW composite longitudinal mode resonator(CLMR) filters and their applications to new synthezised resonator filters", in *Proc. 1993 IEEE Ultrasonics Symposium*, pp. 47–51 (1993).

[87] Y. Yamamoto, R. Kajihara, and S. Yoshimoto, "SAW synthesized resonator filters with two longitudinal mode 2-port resonators", in *Proc. 1998 IEEE Ultrasonics Symposium*, pp. 91–95 (1998).

[88] C. K. Campbell, "Scattering and transmission matrix analysis of SAW resonator filters with long-pair IDTs and triple composite longitudinal modes on quartz", in *Proc. of the 1994 IEEE Ultrasonics Symposium*, pp. 309–312 (1994).

[89] K. M. Lakin, "Electrode resistance effects in interdigital transducers", *IEEE Trans. Microwave Theory Tech.* **22**, pp. 418–424 (1974).

[90] G. Kovacs, W. Sauer, and T. Bauer, "DMS filter with reduced resistive losses", in *Proc. of the 2004 IEEE Ultrasonics Symposium*, pp. 294–297 (2004).

[91] H. A. Haus, "Bulk scattering loss of SAW grating cascades", *IEEE Trans. Sonics Ultrason.* **24**, pp. 259–267 (1977).

[92] M. N. Islam, H. A. Haus, and J. Melngailis, "Bulk radiation by surface acoustic waves propagating under a grating", *IEEE Trans. Sonics Ultrason.* **31**, pp. 123–135 (1984).

[93] K. C. Wagner, L. Reindl, and O. Männer, "Surface wave to bulk wave conversion in SAW-reflectors on strong coupling substrates", in *Proc. of the 1993 Ultrasonics Symposium*, pp. 209–213 (1993).

[94] K. Honkanen, J. Koskela, V. P. Plessky, and M. M. Salomaa, "Parasitic BAW excitation in LSAW transducers", in *Proc. of the 1998 IEEE Ultrasonics Symposium*, pp. 949–952 (1998).

[95] Y. Sakamoto, K. Hashimoto, and M. Yamaguchi, "Behaviour of leaky surface acoustic wave propagation at discontinuous region of periodic grating", *Jpn. J. Appl. Phys.* **37**, pp. 2905–2908 (1998).

[96] Y. Ebata, "Suppression of bulk-scattering loss in SAW resonator with quasi-constant acoustic reflection periodicity", in *Proc. of the 1988 Ultrasonics Symposium*, pp. 91–96 (1988).

[97] W. Wang, X. Zhang, Y. Shui, H. Wu, D. Zhang, and V. P. Plessky, "Minimizing the bulk scattering loss in CRF(DMS) devices", in *Proc. 2004 IEEE Ultrasonics Symposium*, pp. 1363–1366 (2004).

[98] J. V. Knuuttila, P. T. Tikka, C. S. Hartmann, V. P. Plessky, and M. M. Salomaa, "Anomalous asymmetric acoustic radiation in low-loss SAW filters", *Electron. Lett.* **35**, pp. 1115–1116 (1999).

[99] J. Koskela, J. V. Knuuttila, P. T. Tikka, M. M. Salomaa, C. S. Hartmann, and V. P. Plessky, "Acoustic leakage mechanism for leaky SAW resonators on lithium tantalate", *Appl. Phys. Lett.* **75**, pp. 2683–2685 (1999).

[100] J. Koskela, J. V. Knuttila, T. Makkonen, V. P. Plessky, and M. M. Salomaa, "Acoustic loss mechanisms in leaky SAW resonators on lithium tantalate", in *Proc. of the 2000 IEEE Ultrasonics Symposium*, pp. 209–213 (2000).

[101] J. Koskela, J. V. Knuuttila, T. Makkonen, V. P. Plessky, and M. M. Salomaa, "Acoustic loss mechanisms in leaky SAW resonators on lithium tantalate", *IEEE Trans. Ultrason., Ferroelect., Freq. Contr.* **48**, pp. 1517–1526 (2001).

[102] J. Heighway, S. N. Kondratyev, and V. P. Plessky, "Impedance element SAW filters", in *Proc. of the 1994 IEEE International Frequency Control Symposium*, pp. 374–378 (1994).

[103] V. P. Plessky, S. N. Kondratiev, and C. Lambert, "Reduced passband ladder type SAW impedance element filters on strong piezoelectric substrates", in *Proc. of the 1996 IEEE Ultrasonics Symposium*, pp. 11–14 (1996).

[104] C. Vale, J. Rosenbaum, S. Horwitz, S. Krishnaswamy, and R. Moore, "FBAR filters at GHz frequencies", in *Proc. of the 1990 IEEE Frequency Control Symposium*, pp. 332–336 (1990).

[105] M. Ylilammi, J. Ellä, M. Partanen, and J. Kaitila, "Thin film bulk acoustic wave filter", *IEEE Trans. Ultrason., Ferroelect., Freq. Contr.* **49**, pp. 535–539 (2002).

[106] R. Ruby, P. Bradley, D. Clark, D. Feld, T. Jamneala, and K. Wang, "Acoustic FBAR for filters, duplexers and front end modules", in *2004 IEEE MTT-S International Microwave Symposium Digest*, pp. 931–934 (2004).

[107] R. B. Stokes and J. D. Crawford, "X-band thin film acoustic filters on GaAs", in *1992 IEEE MTT-S International Microwave Symposium Digest*, pp. 157–160 (1992).

[108] M. Koshino, K. Kanasaki, N. Akahori, M. Kawase, R. Chujyo, and Y. Ebata, "A wide-band balanced SAW filter with longitudinal multi-mode resonator", in *Proc. 2000 IEEE Ultrasonics Symposium*, pp. 387–390 (2000).

[109] M. Koshino, H. Kanasaki, T. Yamashita, S. Mitobe, M. Kawase, Y. Kuroda, and Y. Ebata, "Simulation modeling and correction method for balance performance

of RF SAW filters", in *Proc. 2002 IEEE Ultrasonics Symposium*, pp. 301–305 (2002).

[110] S. Ichikawa, H. Kanasaki, N. Akahori, M. Koshino, and Y. Ebata, "Mode analysis of longitudinal multi mode SAW resonator filter", in *Proc. 2001 IEEE Ultrasonics Symposium*, pp. 101–106 (2001).

[111] S. Inoue, J. Tsutsumi, Y. Iwamoto, T. Matsuda, M. Miura, Y. Satoh, M. Ueda, and O. Ikata, "1.9 GHz range ultra-low-loss and steep cut-off double mode SAW filter for the Rx band in the PCS antenna duplexer", in *Proc. of the 2003 IEEE Ultrasonics Symposium*, pp. 389–392 (2003).

[112] O. Kawachi, S. Mitobe, M. Tajima, T. Yamaji, S. Inoue, and K. Hashimoto, "A low-loss and wide-band DMS filter using pitch-modulated IDT and reflector structures", in *Proc. of the 2004 IEEE Ultrasonics Symposium*, pp. 298–301 (2004).

[113] J. Machui, G. Müller, W. Ruile, L. Reindl, R. Weigel, and P. Russer, "A new low loss SAW filter structure with extremely wide bandwidth for mobile communications systems", in *1993 IEEE International Microwave Symposium Digest*, pp. 1501–1504 (1993).

[114] G. Müller, J. Machui, L. Reindl, R. Weigel, and P. Russer, "Design of a low loss SAW resonator filter with extremely wide bandwidth for mobile communication systems", *IEEE Trans. Microwave Theory Tech.* **41**, pp. 2147–2155 (1993).

[115] A. N. Rusakov, J. D. Dai, and R. J. Kansy, "Design of wide band SAW coupled resonator filters on quartz", in *Proc. 2003 IEEE Ultrasonics Symposium*, p. 2003 (2003).

[116] H. Nakamura, S. Tsuzuki, T. Yamada, and T. Ishizaki, "An analysis and improvement of balanced-type SAW filters", in *Proc. of the 2002 IEEE Ultrasonics Symposium*, pp. 163–166 (2002).

[117] P. J. Edmonson and C. K. Campbell, "Effect of stray coupling on the balance of a differential LSAW front-end resonator-filter for wireless/mobile circuits", in *Proc. of the 1999 IEEE Ultrasonics Symposium*, pp. 361–364 (1999).

[118] M. A. Sharif, M. A. Schwab, D. P. Chen, and C. S. Hartmann, "Coupled resonator filters with differential input and/or output", in *Proc. of the 1995 IEEE Ultrasonics Symposium*, pp. 67–70 (1995).

[119] Y. Fujita, T. Shiba, S. Kondo, N. Matsuura, M. Hikita, and S. Ogawa, "Low loss and high rejection RF SAW filter using improved design techniques", in *Proc. of the 1998 IEEE Ultrasonics Symposium*, pp. 399–402 (1998).

[120] K. Hashimoto, T. Omori, and M. Yamaguchi, "Design considerations on wide-band longitudinally-coupled double-mode SAW filters", in *Proc. of the 2002 IEEE Ultrasonics Symposium*, pp. 153–157 (2002).

[121] K. Hashimoto, T. Omori, and M. Yamaguchi, "Design considerations on surface acoustic wave resonators with significant internal reflections in interdigital transducers", *IEEE Trans. Ultrason., Ferroelect., Freq. Contr.* **51**, pp. 1394–1403 (2004).

[122] J. Koskela, V. P. Plessky, and M. M. Salomaa, "Suppression of the leaky SAW attenuation with heavy mechanical loading", *IEEE Trans. Ultrason., Ferroelect., Freq. Contr.* **45**, pp. 439–449 (1998).

[123] R. T. Smith and F. S. Wels, "Temperature dependence of the elastic, piezoelectric, and dielectric constants of lithium tantalate and lithium niobate", *J. Appl. Phys.* **42**, pp. 2219–2230 (1971).

[124] T. Yamada, H. Iwasaki, and N. Niizeki, "Piezoelectric and elastic properties of $LiTaO_3$: Temperature characteristics", *Jpn. J. Appl. Phys.* **8**, pp. 1127–1132 (1969).

[125] T. Bauer, G. Kovacs, U. Rösler, and W. Ruile, "Surface acoustic wave arrangement with a junction region between surface acoustic wave structures having a decreasing then increasing finger period", U.S. Patent 6 420 946, July 16, 2002.

[126] M. Hiramoto, "Surface acoustic wave resonator filter with longitudinally coupled resonators having specific resonance frequency placements", U.S. Patent 5 909 158, June 1, 1999.

[127] Y. Takamine, "Longitudinally coupled resonator type surface acoustic wave filter with an IDT having a narrow pitch portion", U.S. Patent 6 583 691, June 24, 2003.

[128] Y. Takamine, "Longitudinally coupled resonator type surface acoustic wave filter having narrow electrode finger pitch sections", U.S. Patent 6 621 380, Sept. 16, 2003.

[129] K. Hashimoto, T. Omori, and M. Yamaguchi, "Operation mechanism of double-mode surface acoustic wave filters with pitch-modulated IDTs and reflectors", in *Proc. of the 2005 IEEE Ultrasonics Symposium*, pp. 2157–2161 (2005).

[130] S. Beaudin, S. Damphousse, and T. Cameron, "Shoulder suppressing technique for dual mode SAW resonators", in *Proc. of the 1999 IEEE Ultrasonics Symposium*, pp. 389–393 (1999).

[131] C. K. Campbell and P. J. Edmonson, "Modeling a longitudinally coupled dual-mode leaky-SAW resonator filter with enhanced upper-sideband suppression", *IEEE Trans. Ultrason., Ferroelect., Freq. Contr.* **48**, pp. 1298–1301 (2001).

[132] G. Fischerauer, D. Gogl, R. Weigel, and P. Russer, "Investigation of parasitic effects in multi-transducer SAW RF filters", in *Proc. of the 1994 IEEE Ultrasonics Symposium*, pp. 241–244 (1994).

[133] T. Makkonen, V. P. Plessky, S. Kondratiev, and M. M. Salomaa, "Electromagnetic modeling of package parasitics in SAW-duplexer", in *Proc. of the 1996 IEEE Ultrasonics Symposium*, pp. 29–32 (1996).

[134] C. Finch, X. Yang, T. Wu, and B. Abbott, "Full-wave analysis of RF SAW filter packaging", in *Proc. of the 2001 IEEE Ultrasonics Symposium*, pp. 81–84 (2001).

[135] C. S. Hartmann, D. T. Bell Jr., and R. C. Rosenfeld, "Impulse model design of acoustic surface-wave filters", *IEEE Trans. Microwave Theory Tech.* **21**, pp. 162–175 (1973).

[136] N. Finger, G. Kovacs, J. Schöberl, and U. Langer, "Accurate FEM/BEM-simulation of surface acoustic wave filters", in *Proc. of the 2003 IEEE Ultrasonics Symposium*, pp. 1680–1685 (2003).

[137] J. Koskela, J. Fegerholm, D. P. Morgan, and M. M. Salomaa, "Self-consistent analysis of arbitrary 1D SAW transducers", in *Proc. of the 1996 IEEE Ultrasonics Symposium*, pp. 135–138 (1996).

[138] C. C. W. Ruppel, W. Ruile, G. Scholl, K. C. Wagner, and O. Männer, "Review of models for low-loss filter design and applications", in *Proc. 1994 IEEE Ultrasonics Symposium*, pp. 313–324 (1994).

[139] C. S. Hartmann, P. V. Wright, R. J. Kansy, and E. M. Garber, "An analysis of SAW interdigital transducers with internal reflections and the application to the

design of single-phase unidirectional transducers", in *Proc. of the 1982 Ultrasonics Symposium*, pp. 40–45 (1982).

[140] C. S. Hartmann and B. P. Abbott, "A generalized impulse response model for SAW transducers including effects of electrode reflections", in *Proc. of the 1988 Ultrasonics Symposium*, pp. 29–34 (1988).

[141] P. V. Wright, "A new generalized modeling of SAW transducers and gratings", in *Proc. of the 43rd Annual Symposium on Frequency Control*, pp. 596–605 (1989).

[142] P. V. Wright, "Analysis and design of low-loss SAW devices with internal reflections using coupling-of-modes theory", in *Proc. 1989 IEEE Ultrasonics Symposium*, pp. 141–152 (1989).

[143] V. P. Plessky and J. Koskela, "Coupling-of-modes analysis of SAW devices", *Int. J. High Speed El. and Syst.* **10**, pp. 867–947 (2000).

[144] B. P. Abbott, C. S. Hartmann, and D. C. Malocha, "A coupling-of-modes analysis of chirped transducers containing reflective electrode geometries", in *Proc. of the 1989 Ultrasonics Symposium*, pp. 129–134 (1989).

[145] B. P. Abbott, "A derivation of the coupling-of-modes parameters based on the scattering analysis of SAW transducers and gratings", in *Proc. of the 1991 Ultrasonics Symposium*, pp. 5–10 (1991).

[146] D. P. Morgan, "Approximate analysis of SAW longitudinally-coupled resonator (LCR) filters", in *Proc. of the 2003 IEEE Ultrasonics Symposium*, pp. 711–714 (2003).

[147] G. Kovacs, "A generalized P-matrix model for SAW filters", in *Proc. of the 2003 IEEE Ultrasonics Symposium*, pp. 707–710 (2003).

[148] Priyanka, S. D. Joshi, and B. S. Panwar, "An iterative approach to design a SAW filter having desired response", *IEEE Trans. Ultrason., Ferroelect., Freq. Contr.* **52**, pp. 1422–1426 (2005).

[149] G. Scholl, A. Christ, W. Ruile, P. H. Russer, and R. Weigel, "Efficient analysis tool for coupled-SAW-resonator filters", *IEEE Trans. Ultrason., Ferroelect., Freq. Contr.* **38**, pp. 243–251 (1991).

[150] D. P. Chen, S. Jen, and C. S. Hartmann, "Resonant modes in coupled resonator filters and the unique equivalent circuit representation", in *Proc. of the 1995 IEEE Ultrasonics Symposium*, pp. 59–62 (1995).

[151] D. P. Morgan, "Idealized analysis of SAW longitudinally coupled resonator filters", *IEEE Trans. Ultrason., Ferroelect., Freq. Contr.* **51**, pp. 1165–1170 (2004).

[152] H. A. Haus and W. Huang, "Coupled-mode theory", *Proc. IEEE* **79**, pp. 1505–1518 (1991).

[153] S. V. Biryukov, G. Martin, V. G. Polevoi, and M. Weihnacht, "Derivation of COM equations using the surface impedance method", *IEEE Trans. Ultrason., Ferroelect., Freq. Contr.* **42**, pp. 602–611 (1995).

[154] R. B. Brown, B. H. Horine, and J. H. Hines, "Practical implementation of coupling-of-modes theory for SAW device modeling", in *Proc. of the 1989 Ultrasonics Symposium*, pp. 153–158 (1989).

[155] V. P. Plessky, "A two parameter coupling-of-modes model for shear horizontal type SAW propagation in periodic gratings", in *Proc. of the 1993 Ultrasonics Symposium*, pp. 195–200 (1993).

[156] V. P. Plessky, D. P. Chen, and C. S. Hartmann, "'Patch' improvements to COM model for leaky waves", in *Proc. of the 1994 Ultrasonics Symposium*, pp. 297–300 (1994).

[157] K. Hashimoto, G. Endoh, and M. Yamaguchi, "Coupling-of-modes modelling for fast and precise simulation of leaky surface acoustic wave devices", in *Proc. of the 1995 IEEE Ultrasonics Symposium*, pp. 251–256 (1995).

[158] B. P. Abbott and K. Hashimoto, "A coupling-of-modes formalism for surface transverse wave devices", in *Proc. of the 1995 IEEE Ultrasonics Symposium*, pp. 239–245 (1995).

[159] K. Hirota and Y. Yamamoto, "Considerations on coupling-of-modes equations for shear horizontal type SAW", in *Proc. of the 2004 IEEE Ultrasonics Symposium*, pp. 2031–2035 (2004).

[160] C. S. Hartmann and B. G. Secrest, "End effects in interdigital surface wave transducers", in *Proc. of the 1972 Ultrasonics Symposium*, pp. 413–416 (1972).

[161] V. I. Grigorievsky and V. P. Plessky, "Extended P-matrix model to calculate imbalance characteristics of CRF filters", in *Proc. of the 2004 IEEE Ultrasonics Symposium*, pp. 1910–1913 (2004).

[162] G. Tobolka, "Mixed matrix representation of SAW transducers", *IEEE Trans. Sonics Ultrason.* **26**, pp. 426–428 (1979).

[163] K. Hashimoto and M. Yamaguchi, "General-purpose simulator for leaky surface acoustic wave devices based on coupling-of-modes theory", in *Proc. of the 1996 IEEE Ultrasonics Symposium*, pp. 117–122 (1996).

[164] K. Hashimoto, *Surface Acoustic Wave Devices in Telecommunications: Modelling and Simulation.* Berlin: Springer-Verlag, 2000, ch. 7, pp. 227–230.

[165] E. K. P. Chong and S. H. Zak, *An Introduction to Optimization.* New York: J. Wiley & Sons, 1996.

[166] D. Quagliarella, J. Périaux, C. Poloni, and G. Winter, Eds., *Genetic Algorithms and Evolutions Strategies in Engineering and Computer Science: Recent Advances and Industrial Applications.* New York: J. Wiley & Sons, 1998.

[167] H.-G. Beyer, *The Theory of Evolution Strategies.* Berlin: Springer-Verlag, 2001.

[168] H.-P. Schwefel, *Evolution and Optimum Seeking.* Chichester: J. Wiley & Sons, 1995.

[169] D. B. Fogel, "An introduction to simulated evolutionary optimization", *IEEE Trans. Neural Networks* **5**, pp. 3–14 (1994).

[170] C. C. W. Ruppel, A. A. Sachs, and F. J. Seifert, "A review of optimization algorithms for the design of SAW transducers", in *Proc. of the 1991 IEEE Ultrasonics Symposium*, pp. 73–83 (1991).

[171] J. Döring and H.-J. Fröhlich, "SAW transducer optimization by the evolutionary computation", in *Proc. 1994 IEEE Ultrasonics Symposium*, pp. 237–240 (1994).

[172] J. Franz, C. C. W. Ruppel, F. Seifert, and R. Weigel, "Hybrid optimization techniques for the design of SAW-filters", in *Proc. 1997 IEEE Ultrasonics Symposium*, pp. 33–36 (1997).

[173] H. Hofmann, H. Stab, and S. Komarov, "Design of SAW correlation devices with evolutionary strategy methods (EVCOR)", in *Proc. of the IEEE 1997 Ultrasonics Symposium*, pp. 171–174 (1997).

[174] K. Tagawa, T. Yamamoto, T. Igaki, and S. Seki, "An Imanishian genetic algorithm for the optimum design of surface acoustic wave filter", in *Proc. 2003 Congress on Evolutionary Calculation*, pp. 2748–2755 (2003).

[175] K. Tagawa, M. Masuoka, and M. Tsukamoto, "Robust optimization design of SAW filters with the Taguchi method and a memetic algorithm", in *Proc. of the 2005 IEEE Congress on the Evolutionary Computation*, pp. 2146–2153 (2005).

[176] K. Tagawa, K. Tokunaga, H. Haneda, T. Igaki, and S. Seki, "Optimal design of three-IDT type SAW filter using local search", in *Proc. of the IEEE 2002 28th Annual Conference of the Industrial Electronics Society*, pp. 2572–2577 (2002).

[177] K. Tagawa, T. Ohtani, T. Igaki, and S. Seki, "Robust optimization design of SAW filters by using penalty function method", in *Proc. of the 2004 IEEE International Conference in Industrial Technology*, pp. 751–756 (2004).

[178] S. Goto and T. Kawakatsu, "Optimization of the SAW filter design by immune algorithm", in *Proc. of the 2004 IEEE International Ultrasonics, Ferroelectrics, and Frequency Control Joint 50th Anniversary Conference*, pp. 600–603 (2004).

[179] V. Prabhu, B. S. Panwar, and Priyanka, "Linkage learning genetic algorithm for the design of withdrawal weighted SAW filters", in *Proc. 2002 IEEE Ultrasonics Symposium*, pp. 357–360 (2002).

[180] N. Hansen and A. Ostermeier, "Adapting arbitrary normal mutation distributions in evolution strategies: The covariance matrix adaptation", in *Proc, of the 1996 IEEE Conference on Evolutionary Computation*, pp. 312–317 (1996).

[181] V. P. Plessky, T. Thorvaldsson, and S. N. Kondratiev, "Degenerated coupled resonator filters", in *Proc. 1996 IEEE Ultrasonics Symposium*, pp. 25–28 (1996).

[182] J. V. Knuuttila, P. T. Tikka, and M. M. Salomaa, "Scanning Michelson interferometer for imaging surface acoustic wave fields", *Opt. Lett.* **25**, pp. 613–615 (2000).

[183] V. I. Grigorievski, Private communication.

Abstracts of Publications I–VI

I The concept of coupled resonators is applied to synthesize surface-acoustic-wave filters. Employing two parallel-connected filter tracks, with a frequency shift imposed between them, a wide passband with low insertion loss together with well-controlled rejections is achieved. The operation of the two-track device is based on the mutual interaction of the individual transfer functions for the pair of tracks. Each track serves to contribute a part of the passband, enabling a wide band. Outside of the passband, the signals passing through the two channels may cancel each other, thus facilitating efficient control over the rejections. However, obtaining rejection stopbands at just the predetermined frequencies requires precise values for the materials parameters and a reliable fabrication process.

Prototype devices fabricated with this approach are demonstrated both on quartz and – for the first time – on 42°-$LiTaO_3$. Results for two-track devices having either two or three transducers per track and operating either single-ended or with a balanced output are presented. The devices are designed employing the coupling-of-modes model and transmission-matrix approach, and the separate tracks are optimized simultaneously and independently. The center frequencies are 868 MHz and 1960 MHz. On quartz, a minimum insertion loss of 4 dB and a passband width of 0.23% are achieved at 868 MHz. On 42°-$LiTaO_3$, the corresponding figures of merit are 1.3 dB for minimum insertion loss and 4.1% bandwidth at 1960 MHz. The filters on 42°-$LiTaO_3$ also have remarkably flat passbands.

II Longitudinally coupled resonator filters provide unbalanced-balanced operation with wide bandwidth, low loss and high suppression levels. However, reducing the insertion loss in the 1.8-2.2 GHz range remains a challenging problem because at high frequencies the resistive losses arising from the relatively wide aperture of the filter may degrade the performance. A 5-interdigital transducer (IDT) filter has six gaps at which the periodicity of the grating is broken, resulting in additional loss due to scattering into the bulk. In this paper, we show that replacing the gaps between the transducers with short transducer sections having their pitch different from that of the main transducers reduces the insertion loss of the device. We present devices with balun operation at 1842 MHz with wide bandwidth of 4.5% and -40 dB suppression, with a minimum insertion loss less than 1 dB in the best devices, and a maximum insertion loss of -1.2 dB in the passband. The passband is quite flat, with < 1 dB ripple. We also discuss the layout of the contact pads and the connections and its effect on the device performance and balance characteristics.

III We study two stochastic optimization algorithms, a genetic algorithm and an evolution strategy, in the context of surface acoustic wave (SAW) filter design. The main reason for employing stochastic methods is to avoid converging to a local minimum of the objective function. As an example we apply these methods to the design of longitudinally coupled SAW filters. As a test structure, we use a symmetric filter structure with 14 simultaneously optimized parameters. We discuss the algorithms and the effect of the main parameters governing the optimization in each case, giving recommendations for parameter values when possible, and compare the performance of the algorithms when applied to the test structure. We demonstrate that the evolution strategy results in more efficient search of combination of variables than the corresponding genetic algorithm.

IV A novel surface acoustic wave filter on a leaky-wave substrate is studied. It features a hiccup-type resonance occurring around a distributed gap between two long interdigital transducers. Compared to a classical coupled resonator filter, it enables a relatively narrow passband (1% to 2% of center frequency) with low insertion loss, steep skirts and improved suppression levels. The structure consists of long transducers having the number of fingers greater than $1/K^2$ and $1/\kappa$, where K^2 is the coupling coefficient of the substrate material and κ is the reflectivity per wavelength, separated with short transducer sections constituting a distributed gap. A strong, localized resonance is formed in the gap region, in addition to the resonance arising in the long structures – hence the name "double-resonance filter". The substrate studied here is 42°-rotated lithium tantalite. We show experimental results for both single-ended and unbalanced-to-balanced filters at 1.6 GHz, having a minimum insertion loss of 1.07 dB, suppressions of 30 dB and absolute −3-dB bandwidth of 29 MHz (1.9% of the center frequency). For the balanced device, the amplitude imbalance over the passband ranges from −0.6 dB to 2 dB and the phase imbalance from 1° to 4.5°. Furthermore, we have measured the acoustical power distributions using a scanning laser interferometer, and compare these results with the profiles simulated using a coupling-of-modes model.

V Radiation of acoustic waves from the contact electrodes (busbars) of surface acoustic wave (SAW) devices on high-coupling piezoelectric substrates, such as 42°-$LiTaO_3$, is demonstrated both with Finite-Element-Method (FEM) simulations and with experimental data. This radiation significantly decreases the Q-value of the busbars. Experimental measurements on test structures show Q-values as low as about 10.

VI We study non-synchronous resonator structures on leaky-wave 42°-$LiTaO_3$ substrate. Such resonators have the resonance frequency in the center of the grating stopband where the reflectors effectively confine the acoustic energy inside the transducer. This can yield improved performance in the form of increased quality factors and reduced ripple. Two structures are presented: a double-resonance device in which a hiccup-type resonance arises with amplitude distribution concentrated around a distributed gap, and a non-synchronous short resonator with transducer pitch smaller than that of the reflectors. Experimental data for both device types are presented, and the possibility of using them as impedance elements in filter applications is briefly discussed.

ISBN-13 978-951-22-8516-7
ISBN-10 951-22-8516-9
ISBN-13 978-951-22-8517-4 (PDF)
ISBN-10 951-22-8517-7 (PDF)
ISSN 1795-2239
ISSN 1795-4584 (PDF)